Heliyon

Received:
10 August 2018
Revised:
16 November 2018
Accepted:
30 November 2018

Cite as: Poornima Devi, Shaheen Fatma, Shraddha Shukla, Roop Kumar, Vineeta Singh, Abha Bishnoi. Synthesis, spectroscopic investigation, molecular docking and DFT studies of novel (2Z,4Z)-2,4-bis(4-chlorobenzylidene)-5-oxo-1-phenylpyrrolidine-3-carboxylic acid (BCOPCA). Heliyon 4 (2018) e01009.
doi: 10.1016/j.heliyon.2018.e01009

Synthesis, spectroscopic investigation, molecular docking and DFT studies of novel (2Z,4Z)-2,4-bis(4-chlorobenzylidene)-5-oxo-1-phenylpyrrolidine-3-carboxylic acid (BCOPCA)

Poornima Devi [a], **Shaheen Fatma** [b], **Shraddha Shukla** [a], **Roop Kumar** [a], **Vineeta Singh** [c], **Abha Bishnoi** [a,*]

[a] *Department of Chemistry, University of Lucknow, Lucknow 226007, India*

[b] *Department of Chemistry, Shri Ramswaroop Memorial University, Lucknow Dewa Road, Barabanki 225003, India*

[c] *Department of Biotechnology, Institute of Engineering and Technology, Lucknow 226021, India*

[*] Corresponding author.

E-mail addresses: abhabishnoi5@gmail.com, dr.abhabishnoi@gmail.com, kushwahapoornima@gmail.com (A. Bishnoi).

Abstract

The synthesized compound **(2Z,4Z)-2,4-bis(4-chlorobenzylidene)-5-oxo-1-phenylpyrrolidine-3-carboxylic acid (BCOPCA)** was characterised by Ultraviolet, FT-Infra Red, ^{1}H, ^{13}C Nuclear Magnetic Resonance and mass spectroscopy. The compound was further subjected to quantum chemical calculations at the level of density functional theory (DFT) using 6-31G (d,p) basis sets method with B3LYP and CAM-B3LYP hybrid functionals. The intramolecular interactions, polarizability, hyperpolarizability and nonlinear optical properties of the title compound were also incorporated in the study. The total first static hyperpolarizability ($\beta_0 = 19.477 \times 10^{-30}$ and 16.924×10^{-30} esu) value was also computed and indicated the title molecule as an interesting forthcoming NLO

https://doi.org/10.1016/j.heliyon.2018.e01009

material. The other thermodynamic properties (entropy, heat capacity and zero vibrational energy) were also discussed. The study also includes NBO computations, complete vibrational assignments, Mulliken charges, UV−Visible spectral analysis and HOMO−LUMO energies. The regions of low and high electron density were obtained from MESP and ESP maps. The calculated parameters for BCOPCA using aforementioned functions are harmonious with the experimental findings. The *in-vitro* antimicrobial activity and molecular docking studies of BCOPCA were also done and showed a good correlation.

Keyword: Theoretical chemistry

1. Introduction

Nitrogen based five membered heterocycle pyrrolidine, is a reassuring molecule for the design of newer drugs. It is well known from the literature that pyrrolidine, is a pharmaceutically active molecule and exhibits miscellaneous biological activities [1, 2, 3, 4, 5]. In addition, it is also apparent that certain compounds with benzylidene moiety in their structure are also important in the field of medicinal chemistry [6]. As a part of our research on the synthesis and DFT studies of novel heterocyclic molecules [7, 8], in this research article, the writers look forward to contribute a detailed account on the molecular geometry, vibrational assignments, mulliken charges, conformations and electronic features of novel **(2Z, 4Z)-2,4-bis(4-chlorobenzylidene)-5-oxo-1-phenylpyrrolidine-3-carboxylic acid (BCOPCA),** obtained by Claisen-Schmidt reaction of 5-oxo-1-phenylpyrrolidine-3-carboxylic acid **(1)** and p-chlorobenzaldehyde **(2)**. The quantum chemical computations were investigated with the help of two hybrid functionals i.e. B3LYP and CAM-B3LYP using 6-31G (d,p) basis sets. The NBO properties of BCOPCA could be seen due to increasing interest in organic materials as non-linear optical devices which gathers the information about bonding and anti-bonding orbitals, electron affinities, bond energies, vibrational frequencies and geometries of organic compounds. The results obtained from computations establish a good agreement with the experimental results [9, 10, 11, 12, 13, 14].

2. Materials and method

The instrument used to record ^{1}H and ^{13}C-NMR spectra of BCOPCA with chemical shifts values in ppm was Bruker 400 MHz, taking $CDCl_3$ as the solvent and TMS as the internal standard. IR (KBr) and UV (200−500 nm, $CHCl_3$) spectra were recorded on a Perkin-Elmer FT-IR and UV-visible Spectrophotometer instruments. The mass spectrum (DART-MS) of BCOPCA was also recorded with the help of JEOL-AccuTOF JMS-T1100LC Mass spectrometer. 5-oxo-1-phenylpyrrolidine-3-carboxylic acid **(1)** was synthesized with the known procedure [15].

 https://doi.org/10.1016/j.heliyon.2018.e01009

2.1. Synthesis of 4(2Z, 4Z)-2,4-bis(4-chlorobenzylidene)-5-oxo-1-phenylpyrrolidine-3-carboxylic acid (BCOPCA)

5-oxo-1-phenylpyrrolidine-3-carboxylic acid (1) (0.005 mol, 1.025) and p-chlorobenzaldehyde (2) (0.005 mol, 0.705)were refluxed together for 5−8 hrs in 10 mL ethanol in presence of pyridine (1 mL). The product (3) obtained on cooling the reaction mixture was filtered and recrystallized from alcohol (Fig. 1). Yield: ∼56%; M.P. 87−89 °C, R_f value: 0.54, MS, m/z: 449 [Hexane: Ethyl acetate] (8.0:2.0 v/v) as mobile phase.

2.2. Computational details

The various DFT studies on BCOPCA were performed at B3LYP and CAM-B3LYP/6-31G (d,p) hybrid functionals respectively. The optimization of BCOPCA molecule was done with the help of GaussView5.0 and the Gaussian 09 software [16, 17, 18]. GIAO program was used for computing ^{1}H & ^{13}CNMR chemical shifts [19]. The Non Bonding Orbital predictions [20] were implemented at DFT/B3LYP level in further to compare the distinct second order interactions. The TD-DFT was used for Frontier orbital study by implementing IEFPCM model taking $CHCl_3$ as solvent. The molecule BCOPCA was analysed by AIM calculation [21]. For potential energy distribution (PED) calculations vibrational problem was set up in terms of internal coordinates using GAR2PED [22] software.

3. Results and discussion

3.1. Molecular geometry

Fig. 2 shows the structure and atom numbering of BCOPCA. The optimized bond lengths and bond angles of BCOPCA are presented in Table 1. On comparing the experimental data of a similar molecule from the literature with the theoretical values of BCOPCA [23, 24], it is perceived that the values for BCOPCA are slightly larger than the data obtained from the literature.

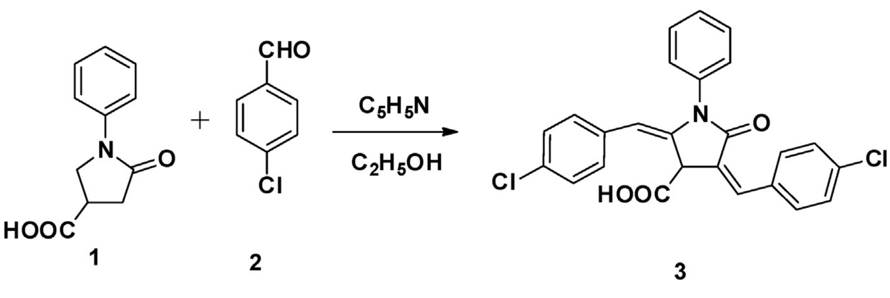

Fig. 1. Synthesis of 4 (2Z,4Z)-2,4-bis(4-chlorobenzylidene)-5-oxo-1-phenylpyrrolidine-3-carboxylic acid (BCOPCA).

https://doi.org/10.1016/j.heliyon.2018.e01009

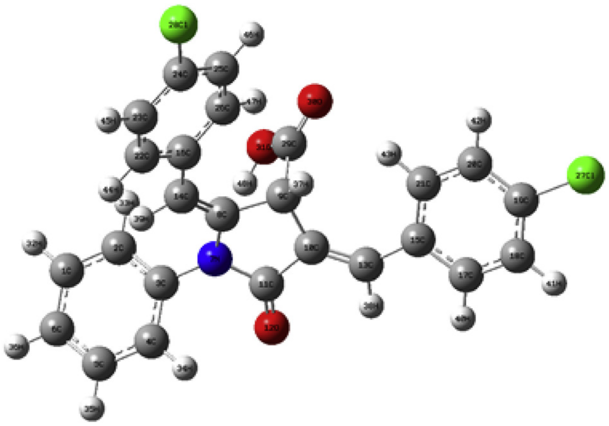

Fig. 2. Optimized structure of BCOPCA.

The bond lengths of two carbonyl groups i.e. C29 = O30 and C11 = O12 and C29-O31 of acid with values of 1.192, 1.215 and 1.282 Å depicted double and single bond characters. The C-C bond lengths of benzene ring of BCOPCA are longer than standard double bond lengths and shorter than the standard single bond lengths ranging from 1.3890 to 1.4591 Å at B3LYP and CAM- B3LYP hybrid functionals. The bond angle value for C2-C1-C6 is found to be 121.5°, revealing slightly distorted hexagonal geometry. The discussed variations may be due to the following reasons: (a) lone pair (b) electronegativity of the central atom and (c) alternate double bonds in BCOPCA.

3.2. Conformational analysis

The Potential Energy Surface (PES) scan (sketched in Fig. 3), performed to determine the most energetically favourable conformer which showed three minima corresponding to the conformers I, II and III with energy values of −2163.74, −2163.76 and −2163.75, a.u. respectively.

3.3. ^{1}H & ^{13}C NMR spectroscopy

Observed and calculated data for ^{1}H and ^{13}C NMR spectra are displayed in Tables 2 and 3. The experimental ^{1}H and ^{13}C NMR spectra of BCOPCA have been measured in $CDCl_3$ and displayed in Fig. 4(a) and (b) respectively. The aromatic ring protons in the ^{1}H NMR spectrum of the title molecule appeared at 7.50−7.53, 7.27−7.33 and 7.06−7.11 ppm respectively. The doublets observed at 7.71−7.74 and 7.86−7.91 ppm represent methine (=CH-) protons and the multiplet at 4.10−4.90 ppm corresponded to pyrrolidine ring. The ^{13}C NMR spectrum showed signals at 172.25 and 171.66 ppm corresponding to carbonyl carbon (−C=O). In BCOPCA signals at 138.51, 131.12, 130.73, 129.21, 128.67, 128.39, 124.70, 124.60 and 119.91 ppm represented the aromatic carbons [25] of phenyl rings. The −CH carbon appeared at 61.36 ppm.

https://doi.org/10.1016/j.heliyon.2018.e01009

Table 1. Optimized geometrical parameters for BCOPCA calculated at B3LYP and CAM-B3LYP as 6-31Gd-p basis sets.

Geometrical parameter calculated with	B3LYP	CAM-B3LYP	Experimental
Bond length (Å)			
C1-C2	1.3931	1.3884	1.3927
C1-C6	1.3965	1.3913	1.381
C1-H32	1.0856	1.0846	0.93
C2-C3	1.4004	1.3926	1.396
C2-H33	1.0856	1.085	0.93
C3-C4	1.3982	1.3912	1.382
C3-N7	1.43	1.428	1.42
C4-C5	1.3949	1.3898	1.38
C4-H34	1.0826	1.0828	0.93
C5-C6	1.3951	1.3904	1.375
C5-H35	1.0856	1.0846	0.93
C6-H36	1.0856	1.0847	0.93
N7-C8	1.424	1.4209	1.472
N7-C11	1.412	1.3955	1.355
C8-C9	1.5212	1.5167	1.525
C8-C14	1.3473	1.3373	0.97
C9-C10	1.5164	1.5125	1.381
C9-C29	1.5475	1.5351	0.93
C9-H37	1.0907	1.0897	1.525
C10-C11	1.486	1.4847	0.97
C10-C13	1.3495	1.3391	0.97
C11-O12	1.2177	1.2142	1.215
C13-C15	1.4591	1.4618	0.93
C13-H38	1.0899	1.0886	1.38
C14-C16	1.4664	1.4685	0.93
C14-H39	1.0868	1.0857	0.93
C15-C17	1.4103	1.402	0.98
C15-C21	1.4105	1.4021	1.523
C16-C22	1.4103	1.4026	1.524
C16-C26	1.4094	1.4013	1.000
C17-C18	1.3895	1.3853	1.390
C17-H40	1.0862	1.0852	1.395
C18-C19	1.3951	1.3886	1.503
C18-C41	1.084	1.0833	1.504
C19-C20	1.3954	1.3887	1.392
C19-Cl27	1.7538	1.7469	1.747

(*continued on next page*)

https://doi.org/10.1016/j.heliyon.2018.e01009

Table 1. (*Continued*)

Geometrical parameter calculated with	B3LYP	CAM-B3LYP	Experimental
C20-C21	1.3913	1.387	1.375
C20-H42	1.0841	1.0834	1.2070
C21-H43	1.0831	1.0825	1.392
C22-C23	1.3901	1.3855	1.207
C22-H44	1.0865	1.0854	1.373
C23-C24	1.3943	1.3883	1.295
C23-H45	1.0842	1.0835	1.207
C24-C25	1.3933	1.3867	1.503
C24-Cl28	1.7574	1.7501	1.264
C25-C26	1.3933	1.3889	1.292
C25-H46	1.0842	1.0836	1.52
C26-H47	1.0826	1.0819	1.371
C29-O30	1.2085	1.2065	1.19
C29-O31	1.3473	1.3372	1.282
O31-H48	0.971	0.97	1.5
Bond angle°			
C2-C1-C6	120.1675	120.0936	121.5
C2-C1-H32	119.552	119.634	119.2
C6-C1-H32	120.2784	120.2706	119.2
C1-C2-C3	119.8525	119.6997	119.9
C1-C2-H33	120.4564	120.5939	120.1
C3-C2-H33	119.6909	119.7062	120.1
C2-C3-C4	120.2038	120.5062	118.4
C2-C3-N7	119.2024	119.1592	119.1
C4-C3-N7	120.5827	120.3336	119.1
C3-C4-C5	119.4649	119.416	120.9
C3-C4-H34	119.8178	119.8271	119.5
C5-C4-H34	120.7059	120.7519	119.5
C4-C5-C6	120.5561	120.3686	121
C4-C5-H35	119.3349	119.496	119.5
C6-C5-H35	120.1088	120.135	119.5
C1-C6-C5	119.7513	119.9117	118.3
C1-C6-H36	120.0944	120.0312	120.8
C5-C6-H36	120.1541	120.057	120.8
C3-N7-C8	124.5285	124.0042	120.4
C3-N7-C11	122.8067	122.5617	127.4
C8-N7-C11	111.7042	111.869	112
N7-C8-C9	106.24	106.1696	103.5

(*continued on next page*)

https://doi.org/10.1016/j.heliyon.2018.e01009

Table 1. (*Continued*)

Geometrical parameter calculated with	B3LYP	CAM-B3LYP	Experimental
N7-C8-C14	123.9764	123.8905	111.1
C9-C8-C14	129.7058	129.8984	111.1
C8-C9-C10	102.7952	102.6542	111.1
C8-C9-29	111.37175	110.8963	111.1
C8-C9-H37	111.7079	111.8358	109
C10-C9-C29	111.1317	110.8401	104.4
C10-C9-H37	113.3464	113.2492	113
C29-C9-H37	106.9355	107.3983	108.1
C9-C10-C11	107.8382	107.5884	114.7
C9-C10-C13	132.5935	132.7076	108.1
C11-C10-C13	119.5053	119.6024	108.1
N7-C11-C10	106.495	106.7195	104.2
N7-C11-O12	125.2761	125.3382	110.9
C10-C11-O12	128.2287	127.9423	110.9
C10-C13-C15	131.9471	131.4343	110.9
C10-C13-H38	113.1128	113.5881	110.9
C15-C13-H38	114.883	114.9079	108.9
C8-C14-C16	130.1969	129.5292	125.2
C8-C14-H39	115.5543	115.9984	125.5
C16-C14-H39	114.1541	114.3742	123.4
C13-C15-C17	117.1306	117.0862	120.2
C13-C15-C21	124.9491	124.6486	116.3
C17-C15-C21	117.92	118.2641	111.1
C14-C16-C22	116.9533	116.9455	113.5
C14-C16-C26	125.6477	125.3662	109.5
C22-C16-C26	117.3968	117.6866	122.7
C15-C17-C18	121.7189	121.5305	120.3
C15-C17-H40	119.1775	119.3283	117.0
C18-C17-H40	119.1009	119.1392	119.0
C17-C18-C19	118.8788	118.7876	120.5
C17-C18-H41	120.8816	120.8289	120.5
C19-C18-H41	120.2393	120.3832	120.0
C18-C19-C20	120.9704	121.178	120.0
C18-C19-Cl27	119.4852	119.4077	120.0
C20-C19-Cl27	119.5417	119.4121	119.8
C19-C20-C21	119.6733	119.5158	123.4
C19-C20-H42	120.0229	120.1268	120.2
C21-C20-H42	120.3005	120.3553	116.3

(*continued on next page*)

https://doi.org/10.1016/j.heliyon.2018.e01009

Table 1. (*Continued*)

Geometrical parameter calculated with	B3LYP	CAM-B3LYP	Experimental
C15-C21C20	120.8245	120.7106	111.1
C15-C21-C43	121.1407	121.2074	113.5
C20-C21-H43	117.9922	118.0484	109.5
C16-C22-C23	121.9783	121.8166	122.7
C16-C22-H44	119.1281	119.2167	120.3
C23-C22-H44	118.8904	118.9649	117.0
C22-C23-C24	119.0437	118.9541	119.0
C22-C23-H45	120.7247	120.6818	120.5
C24-C23-H45	120.2316	120.364	120.5
C23-C24-C25	120.6493	120.851	120.0
C23-C24-Cl28	119.6327	119.5533	120.0
C25-C24-Cl28	119.7147	119.593	120.0
C24-C25-C26	119.7834	119.6139	119.8
C24-C25-H46	120.0714	120.1907	123.4
C26-C25-H46	120.1401	120.1917	109.5
C16-C26-C25	121.1295	121.0607	118.4
C16-C26-H47	121.3002	121.3533	124.3
C25-C26-H47	117.5394	117.5642	124.4
C9-C29-O30	122.9859	123.0089	111
C9-C29-O31	116.4749	116.8521	119.9
O30-C29-O31	120.5385	120.1376	120.1
C29-O31-H48	110.8373	111.9199	120.1
Dihedral angles (°)			
C6-C1-C2-C3	−0.6109	−0.5839	
C6-C1-C2-H33	179.5494	179.5869	
H32-C1-C2-C3	179.9191	179.9014	
H32-C1-C2-H33	0.0794	0.0721	
C2-C1-C6-C5	0.1657	0.2974	
C2-C1-C6-H36	−179.64	−179.6126	−178.80
H32-C1-C6-C5	179.6318	179.809	
H32-C1-C6-H36	−0.1738	−0.1009	
C1-C2-C3-C4	0.5046	0.2642	
C1-C2-C3-N7	179.3026	179.8984	
H33-C2-C3-C4	−179.6545	−179.9051	−178.6
H33-C2-C3-N7	−0.8565	−0.2708	
C2-C3-C4-C5	0.0471	0.3413	
C2-C3-C4-H34	178.8302	179.5328	
N7-C3-C4-C5	−178.7342	−179.2886	

(*continued on next page*)

https://doi.org/10.1016/j.heliyon.2018.e01009

Table 1. (*Continued*)

Geometrical parameter calculated with	B3LYP	CAM-B3LYP	Experimental
N7-C3-C4-H34	0.0489	−0.0971	
C2-C3-N7-C8	57.6483	64.5247	
C2-C3-N7-C11	−134.5078	−130.9131	
C4-C3-N7-C8	−123.5584	−115.8405	
C4-C3-N7-C11	44.2856	48.7217	
C3-C4-C5-C6	−0.4965	−0.6307	
C3-C4-C5-H35	179.6415	179.6003	
H34-C4-C5-C6	−179.2686	−179.8146	
H34-C4-C5-H35	0.8695	0.4164	
C4-C5-C6-C1	0.3921	0.3146	
C4-C5-C6-H36	−179.8023	−179.7755	
H35-C5-C6-C1	−179.7469	−179.9179	
H35-C5-C6-H36	0.0586	−0.0079	
C3-N7-C8-C9	−170.5224	−173.4804	
C3-N7-C8-C14	12.4116	8.6588	
C11-N7-C8-C9	20.4592	20.5093	
C11-N7-C8-C14	−156.6068	−157.3515	
C3-N7-C11-C10	−178.8606	−175.7201	
C3-N7-C11-O12	1.2808	4.2051	
C8-N7-C11-C10	−9.6219	−9.4759	
C8-N7-C11-O12	170.5194	170.4493	
N7-C8-C9-C10	−22.0033	−22.1493	
N7-C8-C9-C29	96.8884	96.2758	
N7-C8-C9-H37	−143.8611	−143.8708	
C14-C8-C9-C10	154.8339	155.536	
C14-C8-C9-C29	−86.2744	−86.039	
C14-C8-C9-H37	32.9761	33.8145	
N7-C8-C14-C16	177.4438	177.3122	
N7-C8-C14-H39	1.234	1.1589	
C9-C8-C14-C16	1.1063	−0.0094	
C9-C8-C14-H39	−175.1036	−176.1627	
C8-C9-C10-C11	16.5817	16.8321	
C8-C9-C10-C13	−160.4262	−159.3659	
C29-C9-C10-C11	−102.2162	−101.6325	
C29-C9-C10-C13	80.7759	82.1695	
H37-C9-C10-C11	137.3216	137.5863	
H37-C9-C10-C13	−39.6863	−38.6117	
C8-C9-C29-O30	129.7818	131.4858	

(*continued on next page*)

https://doi.org/10.1016/j.heliyon.2018.e01009

Table 1. (*Continued*)

Geometrical parameter calculated with	B3LYP	CAM-B3LYP	Experimental
C8-C9-C29-O31	−50.5183	−48.9559	−28.72
C10-C9-C29-O30	−116.4732	−115.1709	−158.40
C10-C9-C29-O31	63.2268	64.3874	19.90
H37-C9-C29-O30	7.7078	9.016	
H37-C9-C29-O31	−172.5923	−171.4257	
C9-C10-C11-N7	−5.2282	−5.4971	
C9-C10-C11-O12	174.6249	174.5803	
C13-C10-C11-N7	172.2412	171.2903	
C13-C10-C11O12	−7.9057	−8.6322	
C9-C10-C13-C15	0.0359	0.1377	
C9-C10-C13-C38	177.0893	176.8905	
C11-C10-C13-C15	−176.6912	−175.6934	
C11-C10-C13-H38	0.3623	1.0595	
C10-C13-C15-C17	165.4828	164.0494	
C10-C13-C15-C21	−14.3457	−15.5468	
H38-C13-C15-C17	−11.5298	−12.6696	
H38-C13-C15-C21	168.6417	167.7342	
C8-C14-C16-C22	−158.5925	−156.846	
C8−14−C16-C26	21.9495	23.6512	
H39-C14-C16-C22	17.6601	19.3583	
H39-C14-C16-C26	−161.7979	−160.1445	
C13-C15-C17-C18	−178.5089	−178.3138	
C13-C15-C17-H40	0.9	1.1686	
C21-C15-C17-C18	1.332	1.309	
C21-C15-C17-H40	−179.2591	−179.2086	
C13-C15-C21-C20	178.7341	178.509	
C13-C15-C21-H43	−3.689	−3.64	
C17-C15-C21-C20	−1.0932	−1.0828	
C17-C15-C21-H43	176.4837	176.7682	
C14-C16-C22-C23	179.0046	179.0529	
C14-C16-C22-C44	−0.3317	−0.4532	
C26-C16-C22-C23	−1.4915	−1.4049	
C26-C16-C22-H44	179.1723	179.0889	
C14-C16-C26-C25	−179.0959	−179.1017	
C14-C16-C26-H47	2.9761	2.6388	
C22-C16-C26-C25	1.4482	1.3988	
C22-C16-C26-H47	−176.4797	−176.8606	
C15-C17-C18-C19	−0.5914	−0.5794	

(*continued on next page*)

https://doi.org/10.1016/j.heliyon.2018.e01009

Table 1. (*Continued*)

Geometrical parameter calculated with	B3LYP	CAM-B3LYP	Experimental
C15-C17-C18-H41	179.5982	179.5994	
C40-C17-C18-C19	179.9992	179.9373	
H40-C17-C18-H41	0.1888	0.1161	
C17-C18-C19-C20	−0.4198	−0.4037	
C17-C18-C19-Cl27	−179.8184	−179.8652	
H41-C18-C19-C20	179.3919	179.4184	
H41-C18-C19-Cl27	−0.0067	−0.0432	
C18-C19-C20-C21	0.6457	0.6179	
C18-C19-C20-H42	−178.702	−178.8638	
Cl27-C19-C20-C21	−179.956	−179.9206	
Cl27-C19-C20-H42	0.6963	0.5977	
C19-C20-C21-C15	0.1344	0.1463	
C19-C20-C21-H43	−177.517	−177.7711	
H42-C20-C21-C15	179.4802	179.6268	
H42-C20-C21-H43	1.8289	1.7093	
C16-C22-C23-C24	0.5254	0.4755	
C16-C22-C23-H45	−179.5588	−179.6161	
H44-C22-C23-C24	179.8632	179.9829	
H44-C22-C23-H45	−0.2211	−0.1087	
C22-C23-C24-C25	0.5332	0.5037	
C22-C23-C24-Cl28	179.8698	179.9084	
H45-C23-C24-C25	−179.383	−179.4049	
H45-C23-C24-Cl28	−0.0463	−0.0003	
C23-C24-C25-C26	−0.5664	−0.5021	
C23-C24-C25-H46	178.6157	178.803	
Cl28-C24-C25-C26	−179.9025	−179.9065	
Cl28-C24-C25-H46	−0.7204	−0.6014	
C24-C25-C26-C16	−0.4575	−0.4786	
C24-C25-C26-H47	177.5459	177.8447	
H46-C25-C26-C16	−179.639	−179.7837	
H46-H25-C26-H47	−1.6357	−1.4604	
C9-C29-O31-H48	1.20772	1.8811	
O30-C29-O31-H48	−179.335	−178.5472	

3.4. Electronic absorption

The UV-Visible spectrum of compound was computed at the B3LYP and CAM-B3LYP hybrid functionals with 6-31G (d,p) basis sets and integral equation formalism polarizable continuum model (IEFPCM) was employed for accounting

https://doi.org/10.1016/j.heliyon.2018.e01009

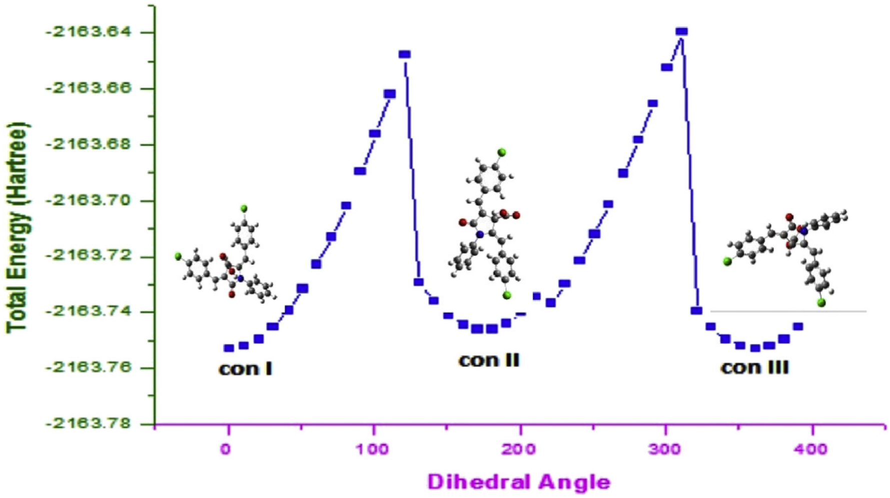

Fig. 3. PES scan for the selected torsional angle T (N7-C8-C14-H39) of freedom.

Table 2. Calculated and experimental [1]H NMR chemical shifts (δ/ppm) of BCOPCA in $CDCl_3$.

	$\delta_{calcd.}$		$\delta_{exp.}$	Assignment
	B3LYP	CAM-B3LYP		
32H	7.36	7.82	7.339−7.062	m, 5H, phenyl ring
33H	8.48	8.63		
34H	7.08	7.3		
35H	7.59	7.76		
36H	7.21	7.35		
37H	8.79	8.76	4.109−3.900	m, 1H, CH in pyrrolidine ring
38H	7.25	7.65	7.742−7.714	m, 2H, CH between pyrrolidine and 4-chloro substituted phenyl ring
39H	6.41	6.63		
40H	7.21	7.49	7.533−7.507	dd, 4H, 4-chloro substituted phenyl ring
41H	7.12	7.36		
42H	7.65	7.9		
43H	10.03	11.43		
44H	6.71	6.93	7.434−7.406	dd, 4H, 4-chloro substituted phenyl ring
45H	7.08	7.3		
46H	7.76	8.09		
47H	4.96	4.04		
48H	7.51	7.45	11.45	Hydroxyl proton of carboxylic acid

solvent effect [26]. The excitation energies, oscillator strength, percent contributions have been tabulated in Table 4. Fig. 5 represents two intense electronic transitions at 348 and 278 with an oscillator strength f = 0.269 and 0.255 in chloroform complying to the observed values of 256 and 240 nm. The title compound depicted

 https://doi.org/10.1016/j.heliyon.2018.e01009

Table 3. Calculated and experimental ^{13}C NMR chemical shifts (δ/ppm) of BCOPCA in $CDCl_3$-solvent.

Atom	$\delta_{calcd.}$		$\delta_{exp.}$	Assignment
	B3LYP	CAM-B3LYP		
1C	129.04	129.11	124.70−119.91	Phenyl ring attached at nitrogen of pyrrolidine ring
2C	117.29	116.65		
3C	126.25	132.85		
4C	115.92	114.78		
5C	127.81	127.81		
6C	120.83	119.99		
8C	88.87	134.71	77.64−76.69	Pyrrolidine ring
9C	135.99	71.17		
10C	73.5	126.74		
11C	130.46	167.93	171.66	C=O in Pyrrolidine ring
13C	167.6	128.88	61.36	Methine group between Pyrrolidine and 4-chloro substituted phenyl ring
14C	127.71	103.11		
15C	102.78	116.93	129.21−128.39	4-chloro substituted phenyl ring
16C	117.88	123.98		
17C	124.37	133.12		
18C	133.09	125.55		
19C	126.2	140.8		
20C	142.34	130.01		
21C	130.56	146.57		
22C	145.77	128.51	138.51−130.73	4-chloro substituted phenyl ring
23C	128.75	129.7		
24C	129.75	134.82		
25C	136.38	128.23		
26C	189.63	188.07		
29C	149.5	149.38	172.25	C=O group in carboxylic acid

n → π* HOMO-1 to LUMO+1 with 63% and π → π* HOMO-2 to LUMO with 53% contribution as shown in Fig. 6. The HOMO-LUMO energy gaps were found to be 2.199 (B3LYP) and 3.060 (CAM-B3LYP).

3.5. Vibrational assignment

There are 48 atoms having C1 point group and 138 routine modes of vibrations performed on the basis of recorded FT-IR spectrum, in BCOPCA. The discard of anharmonicity in real system is responsible for higher calculated vibrational wavenumbers than the observed wavenumbers. Therefore, calculated wavenumbers are scaled

https://doi.org/10.1016/j.heliyon.2018.e01009

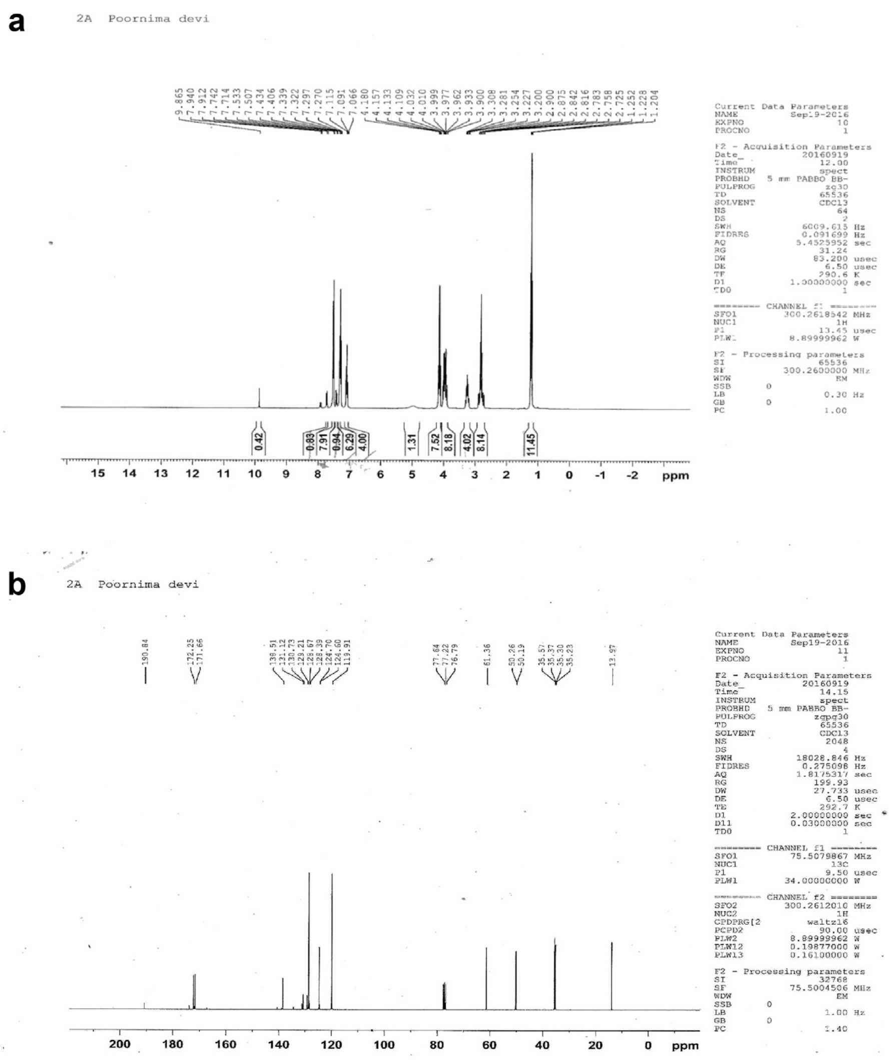

Fig. 4. (a) ^{1}HNMR spectra of BCOPCA. (b) ^{13}HNMR spectra of BCOPCA.

down by a single factor 0.9679 [27] B3LYP and compared with experimental wavenumbers. The observed and computed frequencies, PED and simulated vibrational spectra of BCOPCA are presented in Table 5 and Fig. 7.

The experimental FT-IR -OH stretching vibration band appeared at 3622 cm^{-1} is in good agreement with the calculated value at 3545 cm^{-1} with a contribution of 68% [28, 29, 30, 31]. The band at 2944 cm^{-1} is assigned to C-H stretching vibrations with a calculated value of 3054 cm^{-1} and 86% contribution. The C−H in plane bending vibrations with 63% contribution and out of plane bending vibrations with 41% contribution in IR were observed at 1375, 1038 and 978, 805 cm^{-1} respectively [32, 33, 34]. The bands for C=C and C−C stretching vibrations in the molecule appeared at 1375, 1442, and 1513 cm^{-1} depicting good correlation between theoretical and experimental values [35, 36]. The carbonyl carbons showed stretching

https://doi.org/10.1016/j.heliyon.2018.e01009

Table 4. Experimental and theoretical absorption wavelengths λ (nm) and excitation energies E (eV) of BCOPCA using functional B3LYP and CAM-B3LYP 6-31G/(d,p) basis set.

	Major contributing molecular orbitals	E (eV)	Calculated (λ_{max})	Oscillatory strength (f)	Assignments	Observed (λ_{max})
B3LYP	H → L (69%)	2.19	523	0.014	π → π*	288
	H-1 → L+1 (63%)	2.92	424	0.225	n → π*	273
	H-2 → L (61%)	3.55	348	0.269	π → π*	256
	H-2 → L+2 (46%)	3.77	328	0.222	n → π*	240
	H-4 → L (46%)	3.99	310	0.192	π → π*	227
CAM-B3LYP	H → L (55%)	3.06	405	0.05	π → π*	288
	H-1 → L (40%)	3.49	354	0.40	n →π*	273
	H → L+2 (45%)	3.82	323	0.11	π → π*	256
	H-2 → L (53%)	4.45	278	0.25	n → π*	240
	H-2 → L+1 (52%)	4.65	266	0.14	π → π*	227

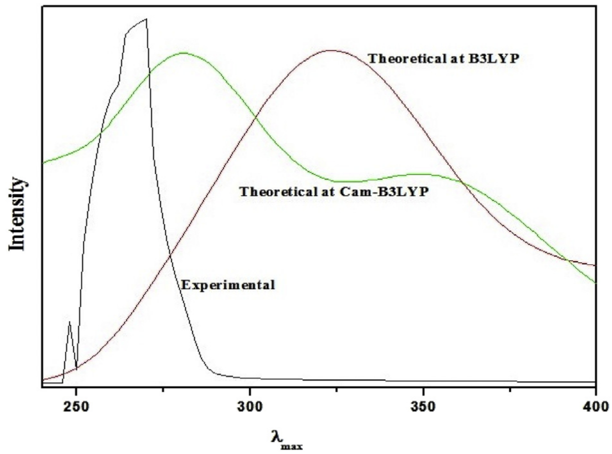

Fig. 5. Experimental and theoretical UV-Visible spectra of BCOPCA.

vibrations at 1729 and 1702 cm^{-1} [37] while it was calculated at 1716 cm^{-1}. The C–O stretching vibration [38, 39] appeared at 1036 cm^{-1} complying well with the calculated value at 1020 cm^{-1}. C-Cl vibration in BCOPCA appeared at 679 cm^{-1} with PED contribution of 53% and is in good agreement with the observed wavenumber at 667 cm^{-1} [40].

3.6. Mulliken charge distribution

The Mulliken charges were calculated at two different levels as enumerated in Table 6 and plotted in Fig. 8. On the basis of the results performed on neutral molecule the negative charges were delocalized on O12, O30 and O31 atoms and similar positive charges were noticed on all the hydrogen atoms in the molecule. C11 and C29 attached with oxygen atoms had more positive charges due to electronegative character of oxygen atoms [41, 42, 43]. Almost like values of positive charges were

 https://doi.org/10.1016/j.heliyon.2018.e01009

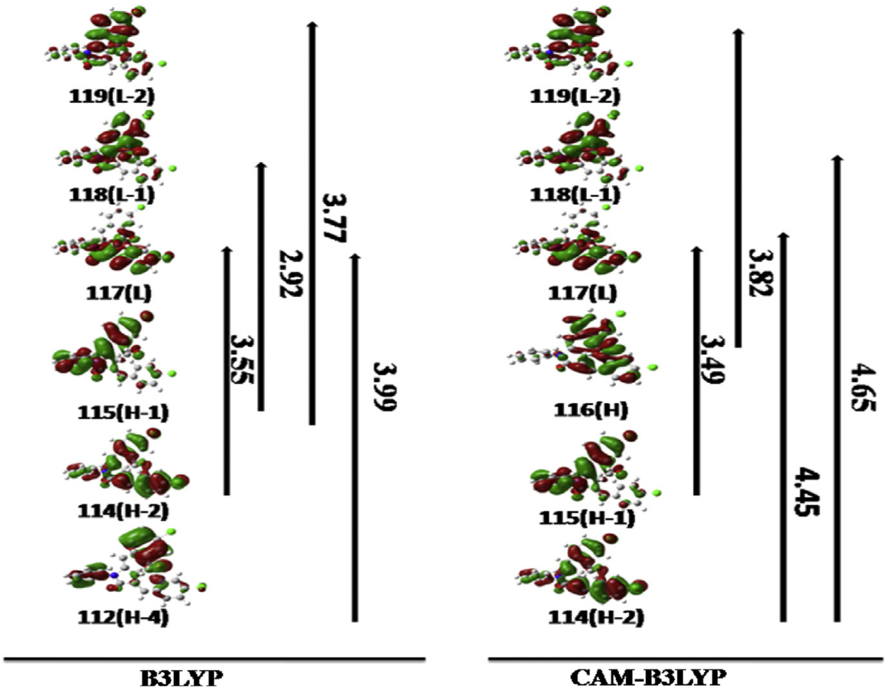

Fig. 6. HOMO-LUMO Transitions of BCOPCA using B3LYP and CAM-B3LYP/6-31-G (d,p) basis sets.

observed for hydrogen atoms bonded to carbon atoms in the aromatic ring. It must be noted that the biggest value of charge on H48 might be due to hydrogen bonding.

3.7. Molecular electrostatic potential

A colour scheme depicting different values of the electrostatic potential in ascending order at the surface is as follows: red < yellow < green < light blue < blue (Figs. 9 and 10). Red colour depicts nucleophilic region while blue depicts electrophilic region [44, 45, 46, 47]. The yellow, green and light blue colours portrayed slightly electron rich; neutral and slightly electron deficient regions respectively [48, 49]. The region of maximum negative electrostatic potential with a value of −7.648 a.u, is around C11 & O12 and the most positive region with a value of +7.648 a.u, is at C47 & O30, as revealed by MEP and ESP maps. C11, O12 and C47, O30 are most preferred sites for nucleophilic and electrophilic attack respectively.

3.8. Non bond orbital (NBO) analysis

The hyperconjugative interactions in molecular systems [50, 51], correlation between donor (i), acceptor (j) level bonds and stabilization energy E(2) are explained according to second order Fock matrix as follows:

https://doi.org/10.1016/j.heliyon.2018.e01009

Table 5. Experimental and calculated (selected) vibrational wavenumbers of BCOPCA using B3LYP/6-31 G (d,p) and their assignments [harmonic wavenumbers (cm^{-1}), IR int ($Kmmol^{-1}$)].

Wave number unscaled	Wave number scaled	Exp. Wave numbers	Exp.IR$_{int}$	Assignment (PED) ≥ 5 %
3689.7	3545.064	3622	101.07	ν(O31-H48) (68.) ν(O22-C20) (41.)
3263.2	3135.283	3297	1.92	ν(C26-H47) (11.)
3241.8	3114.721		4.65	ν(C18-H41) (37.) ν(C5-C6) (32.)
3239.5	3112.512	3205	132.76	ν(C23-H45) (31.)
3235.2	3108.38		11.28	ν(C20-H42) (17.) -ν(C5-C6) (34.)
3223.6	3097.235		26.29	ν(C25-H46) (7.) ν(C25-C26) (14.) -ν(C25-C21) (9.)
3213.5	3087.531		1.83	ν(C5-C36) (17.) -ν(C5-C6) (23.) -ν(C1-C2) (27.)
3187.8	3062.838	3003	33.77	-ν(C6-H36) (34.) -ν(C1-C6) (18.) ν(C5-C6) (14.)
3186.6	3061.685		11.27	ν(C2-C3) (16.) ν(C1-C6) (12.) -ν(C4-H34) (7.) ν(C5-C6) (13.)
3179.2	3054.575	2944	13.35	ν(C5-H35) (86.)
3173.4	3049.003	2893	4.61	ν(C17-H40) (29.) ν(C17-C15) (7.)
3168.3	3044.103		0.44	ν(C22-H44) (16.) ν(C22-C23) (9.) ν(C22-C16) (6.)
3157.08	3033.322		1.99	ν(C6-C36) (51.)
3127.25	3004.662		107.24	ν(C14-H39) (39.) ν(C14-C8) (32.) ν(C16-C14) (19.)
1827.74	1756.093		0.21	ν(C2-C3) (99.)
1786.58	1716.546	1729	11.17	ν(C4- C20) (99.)
1710.14	1643.103	1702	33.06	ν(C4-H34) (60.) ν(C3-N4) (15.) ν(C1-H32) (12.) ν(C1-H32) (6.)
1692.15	1625.818		154.16	ν(C1-C6) (69.) ν(C4-C5) (9.) -ν(C10-C11) (5.)
1652.43	1587.655		9.19	ν(C3-C4) (45.) ν(C1-C2) (12.) -ν(C1-C2) (9.) -ν(C1-C2) (6.) -ν(C2-H33) (5.)
1643.02	1578.614		101.03	ν(C1-C2) (42.) -ν(C3-C4) (11.) -δ(C10-C13-H38) (7.) ν(C1-C6) (7.) -ν(C1-H32) (5.) -ν(C10-C11) (5.)
1641.62	1577.268		135.99	ν(C1-C2) (24.) ν(C4-C5) (22.) -ν(C2-C3) (8.) -ν(C5-C6) (7.) ν(C4-C5) (6.) -ν(C2-C3) (6.) ν(C2-C3) (5.)
1640.94	1576.615		41.78	ν(C22-C23) (23.) ν(C3-C4) (21.) -ν(C4-H34) (12.) -ν(C4-H34) (7.) -ν(C16-C26) (7.) ν(C1-C2) (7.) ν(C2-H33) (5.)
1611.62	1548.444		15.76	ν(C1-C6) (18.) ν(C3-C4) (16.) -ν(C5-C6) (14.) -ν(C2-C3) (12.) -ν(C1-H32) (5.) -ν(C1-C2) (5.) -ν(C3-N4) (5.)

(continued on next page)

https://doi.org/10.1016/j.heliyon.2018.e01009

Table 5. (*Continued*)

Wave number unscaled	Wave number scaled	Exp. Wave numbers	Exp.IR$_{int}$	Assignment (PED) ≥ 5 %
1609.97	1546.859		24.12	ν(C1-C2) (17.) ν(C3-N4) (16.) ν(C1-H32) (8.) -ν(C3-C4) (6.) -ν(C3-N4) (6.) ν(C4-C5) (6.) -ν(C4-C5) (5.)
1539.05	1478.719	1513	11.43	ν(C4-C5) (16.) ν(C2-C3) (15.) ν(C4-H34) (14.) -ν(C1-C2) (14.) -ν(C1-C6) (12.) -ν(C16-C26) (11.) -δ(C8-C14-C16) (6.)
1535.31	1475.126		51.92	ν(C2-H33) (21.) -ν(C1-H32) (17.) -ν(C4-C5) (17.) ν(C3-N4) (14.) -ν(C2-C3) (9.) -ν(C3-C4) (5.)
1533.9	1473.771	1442	183.64	ν(C2-C3) (15.) -δ(C2-C1-H32) (15.) -ν(C4-C5) (14.) ν(C3-C4) (12.) ν(C3-C4) (9.) ν(C2-C3) (9.) -ν(C5-C6) (8.) -ν(C1-C6) (8.) -ν(C3-N4) (7.)
1494.33	1435.752		166.6	ν(C1-H32) (14.) -ν(C3-N4) (13.) ν(C1-C6) (13.) ν(C1-C2) (12.) -ν(C4-H34) (11.) -ν(C4-H34) (11.) ν(C2-C3) (7.) -ν(C16-C26) (5.)
1452.24	1395.312		16.69	δip (C17-H40) (16.) -ν(C2-C3) (15.) ν(C1-H32) (13.) ν(C4-C5) (13.) -ν(C3-C4) (12.) ν(C2-H33) (7.) -ν(C3-N4) (7.) -ν(C4-C5) (5.)
1451.23	1394.342		200.84	ν(C1-C2) (20.) -ν(C4-C5) (19.) -ν(C2-C3) (13.) -δ(C2-C1-H32) (13.) ν(C1-C6) (10.) ν(C2-C3) (6.) -ν(C3-C4) (5.)
1421.23	1365.518		9.5	ν(C1-C2) (22.) -ν(C22-C23) (10.) ν(C3-C4) (10.) ν(C1-C2) (7.) -ν(C4-H34) (7.) -ν(C1-C2) (6.) -ν(C4-C5) (6.)
1404.45	1349.396		6.13	ν(C1-C2) (13.) -ν(C3-N4) (12.) ν(C3-C4) (9.) -ν(C1-C2) (9.) ν(C4-C5) (7.) -δ(C10-C13-H38) (6.) -δip (C17-H40) (5.)
1365.65	1312.117	1375	3.93	ν(C1-C6) (25.) δ(C8-C14-C16) (17.) -ν(C1-C2) (17.) ν(C3-C4) (5.) ν(C2-H33) (5.)
1360.93	1307.582		2.22	δ(C10-C13-H38) (42.) -ν(C3-N4) (11.) -ν(C3-N4) (8.) ν(C3-C4) (5.) ν(C1-C2) (5.)
1347.32	1294.505		31.21	ν(C4-C5) (9.) ν(C1-C2) (8.) -ν(C3-N4) (6.) -δ(C8-C14-C16) (6.) ν(C5-C6) (5.)
1343.19	1290.537		467.5	ν(C3-C4) (13.) δ(C8-C14-C16) (9.) ν(C4-C5) (8.) ν(C1-C6) (6.) ν(C3-N4) (6.) -ν(C4-C5) (5.) ν(C1-C2) (5.)
1338.76	1286.281		7.6	ν(C3-C4) (8.) ν(C2-C3) (7.) -ν(C1-H32) (6.) δip (C17-H40) (6.) -ν(C4-C5) (6.)
1337.4	1284.974		85.78	ν(C2-C3) (13.) -ν(C3-C4) (13.) -ν(C5-C6) (7.) ν(C1-C6) (7.) ν(C2-C3) (6.) -ν(C1-C2) (6.) δ(C2-C1-H32) (6.) -ν(C3-C4) (5.) ν(C4-C5) (5.)
1326.19	1274.203		21.8	ν(C2-C3) (14.) -ν(C1-C6) (12.) ν(C4-H34) (10.) ν(C1-C2) (9.) ν(C1-H32) (7.) -ν(C4-H34) (6.) ν(C3-N4) (5.)

(*continued on next page*)

 https://doi.org/10.1016/j.heliyon.2018.e01009

Table 5. (*Continued*)

Wave number unscaled	Wave number scaled	Exp. Wave numbers	Exp.IR$_{int}$	Assignment (PED) ≥ 5 %
1316.12	1264.528		43.95	ν(C2-H33) (21.) -ν(C1-H32) (18.) ν(C4-C5) (12.) -ν(C3-N4) (11.) ν(C1-C2) (7.) ν(C4-C5) (5.)
1285.83	1235.425		44.82	ν(C4-C5) (14.) -δ(C8-C14-C16) (12.) -ν(C1-C2) (11.) -ν(C16-C26) (8.) ν(C2-H33) (6.) ν(C4-H34) (6.) -ν(C2-C3) (5.)
1276.77	1226.721		104.08	ν(C1-H32) (42.) -ν(C3-N4) (24.) -ν(C29-O31) (13.)
1269.12	1219.37		50.09	ν(C1-H32) (34.) -ν(C3-N4) (34.) -ν(C2-H33) (15.)
1232.16	1183.859		111.88	ν(C2-C3) (19.) -ν(C3-N4) (16.) ν(C1-H32) (15.) -ν(C1-H32) (6.) -ν(C2-H33) (6.) -ν(C3-N4) (5.)
1222.23	1174.319		4.82	ν(C3-N4) (10.) ν(C2-H33) (10.) -ν(C1-H32) (8.) -ν(C1-H32) (8.) δ(C8-C14-C16) (7.) -ν(C4-H34) (7.) ν(C2-C3) (7.) ν(C1-C2) (5.)
1220.82	1172.964		55.32	ν(C2-C3) (27.) ν(C1-H32) (11.) ν(C4-H34) (9.) -ν(C2-H33) (7.) -ν(C3-N4) (7.) ν(C1-C2) (6.)
1206.25	1158.965		34.78	ν(C2-C3) (16.) -ν(C3-C4) (14.) ν(C4-C5) (13.) -δip (C17-H40) (8.) -ν(C3-N4) (7.) ν(C3-N4) (6.) -ν(C3-C4) (5.)
1201.85	1154.737		5.82	ν(C3-N4) (16.) -ν(C4-H34) (13.) ν(C1-C2) (12.) -ν(C1-H32) (10.) -ν(C3-C4) (8.) -ν(C2-C3) (6.) ν(C3-C4) (5.)
1194.19	1147.378		3.6	δ(C2-C1-H32) (23.) -ν(C4-C5) (18.) ν(C3-C4) (16.) -ν(C2-C3) (16.) ν(C1-C2) (11.) ν(C4-C5) (6.)
1186.58	1140.066		3.71	ν(C3-N4) (41.) -ν(C1-H32) (23.) -ν(C29-O31) (9.) -ν(C2-H33) (8.) ν(C4-C5) (5.)
1180.41	1134.138		5.73	ν(C1-C6) (18.) δ(C8-C14-C16) (15.) ν(C2-C3) (11.) -ν(C1-H32) (10.) ν(C4-H34) (5.) -ν(C10-C11) (5.)
1150.05	1104.968		2.92	ν(C2-C3) (32.) δ(C2-C1-H32) (26.) ν(C5-C6) (11.) -ν(C1-C6) (9.)
1146.19	1101.259		0.61	ν(C3-N4) (14.) -ν(C1-H32) (8.) -ν(C10-C11) (8.) -ν(C1-C6) (8.) ν(C1-H32) (8.) -δ(C8-C14-C16) (6.) -ν(C2-H33) (5.)
1125.27	1081.159	1078	0.24	δip (C17-H40) (21.) ν(C1-C2) (14.) ν(C2-C3) (11.) -ν(C4-C5) (9.) -ν(C3-N4) (9.) -ν(C3-C4) (8.) ν(C2-C3) (6.)
1109.35	1065.863	1038	0.94	ν(C1-C2) (25.) -ν(C1-H32) (14.) -ν(C22-C23) (11.) -ν(C3-N4) (7.) -ν(C4-C5) (7.) ν(C3-C4) (6.) ν(C1-C2) (6.) ν(C4-H34) (5.) -ν(C4-H34) (5.)
1108.03	1064.595		5.41	ν(C1-C6) (14.) ν(C3-N4) (13.) -ν(C2-C3) (11.) -ν(C3-C4) (9.) -ν(C10-C11) (5.)

(*continued on next page*)

https://doi.org/10.1016/j.heliyon.2018.e01009

Table 5. (*Continued*)

Wave number unscaled	Wave number scaled	Exp. Wave numbers	Exp.IR$_{int}$	Assignment (PED) ≥ 5 %
1105.37	1062.039		50.09	ν(C1-C2) (9.) -ν(C2-H33) (8.) ν(C1-C6) (8.) ν(C2-C3) (8.) -ν(C4-C5) (7.) ν(C1-H32) (6.) -ν(C3-C4) (5.) ν(C2-H33) (5.) -ν(C3-C4) (5.)
1054.67	1013.327		6.53	ν(C2-H33) (17.) -ν(C1-C6) (16.) -ν(C2-C3) (16.) ν(C1-H32) (7.) -ν(C3-C4) (6.) ν(C2-H33) (6.)
1023.66	983.5325		50.81	ν(C2-H33) (12.) -ν(C3-C4) (11.) ν(C1-H32) (10.) ν(C2-C3) (8.) -ν(C1-C2) (7.)
1021.59	981.5437		21.37	ν(C5-C6) (27.) ν(C1-C6) (26.) -δ(C2-C1-H32) (6.) -ν(C1-C6) (6.) ν(C3-C4) (6.) ν(C2-C3) (5.)
1018.45	978.5268	918	6.43	ν(C1-C6) (63.) ν(C4-C5) (10.) ν(C3-N4) (9.) -ν(C3-C4) (5.)
1005.8	966.3726		32.43	ν(C4-C5) (35.) ν(C4-H34) (17.) ν(C16-C26) (12.) -ν(C4-H34) (11.) -ν(C2-H33) (8.)
1001.41	962.1547		2.27	ν(C1-C6) (63.) ν(C2-C3) (8.) ν(C3-C4) (8.) ν(C4-C5) (6.) ν(C1-C2) (5.)
988.26	949.5202		25.84	ν(C1-H32) (28.) -ν(C2-H33) (19.) ν(C1-C2) (18.) ν(C2-H33) (17.) -ν(C4-H34) (5.)
983.9	945.3311		35.87	ν(C2-H33) (21.) -ν(C3-N4) (11.) ν(C1-C6) (10.) -ν(C3-N4) (6.) ν(C2-H33) (5.)
980.18	941.7569		17.69	ν(C1-C2) (32.) ν(C3-N4) (18.) -ν(C2-H33) (10.) -ν(C4-H34) (10.) ν(C4-H34) (10.) -ν(C2-H33) (9.)
977.39	939.0763		25.74	ν(C3-N4) (21.) -ν(C2-H33) (16.) -ν(C4-H34) (13.) -ν(C1-C2) (13.) -ν(C10-C11) (9.) ν(C1-C2) (7.) ν(C4-C5) (5.) -ν(C3-N4) (5.)
968.88	930.8999		32.85	ν(C10-C11) (38.) -ν(C4-C5) (25.) ν(C3-N4) (7.) -ν(C2-H33) (5.)
963.22	925.4618		9.93	ν(C2-H33) (24.) -ν(C1-C2) (22.) ν(C4-H34) (19.) -ν(C3-N4) (14.) ν(C3-C4) (12.) -ν(C3-N4) (8.)
940.85	903.9687		17.69	ν(C1-C6) (30.) -ν(C2-C3) (23.) -ν(C4-C5) (22.) ν(C5-C6) (20.)
929.51	893.0732		18.41	ν(C1-C2) (33.) ν(C1-C2) (25.) -ν(C4-H34) (22.) ν(C2-H33) (6.)
903.87	868.4383		7.93	ν(C10-C11) (15.) -ν(C4-C5) (8.) ν(C1-C6) (7.) -ν(C4-C5) (6.) ν(C3-N4) (5.)
888.87	854.0263		10.42	ν(C4-H34) (27.) ν(C3-N4) (27.) -ν(C3-N4) (11.) ν(C2-H33) (8.) ν(C1-H32) (7.)
876.45	842.0932		4.24	ν(C1-C6) (49.) -(τ−R2) (10.) ν(C4-C5) (6.)
853.77	820.3022		11.95	(τ−R2) (30.) ν(C1-C6) (11.) -ν(C4-C5) (10.) -ν(C1-H32) (9.) -ν(C29-O31) (8.) -ν(C3-N4) (7.) -δ(C8-C14-C16) (6.)

(*continued on next page*)

 https://doi.org/10.1016/j.heliyon.2018.e01009

Table 5. (*Continued*)

Wave number unscaled	Wave number scaled	Exp. Wave numbers	Exp.IR$_{int}$	Assignment (PED) ≥ 5 %
850.75	817.4006		21.31	δ(C8-C14-C16) (31.) ν(C1-C6) (26.) -ν(C2-H33) (8.) ν(C3-C4) (7.)
847.74	814.5086		19.72	δ(C8-C14-C16) (26.) (τ−R2) (13.)
844.44	811.338		14.39	6ν(C3-N4) (31.) -ν(C4-H34) (26.) -ν(C1-C2) (20.) ν(C2-H33) (16.)
838.36	805.4963	792	11.09	ν(C2-H33) (41.) ν(C3-N4) (23.) -ν(C3-C4) (14.) -ν(C4-H34) (9.)
832.42	799.7891		0.08	ν(C4-C5) (38.) ν(C10-C11) (27.)
800.72	769.3318		9	ν(C1-C2) (41.) ν(C4-H34) (34.) -ν(C3-C4) (10.) -ν(C4-H34) (6.)
789.41	758.4651	749	9.21	ν(C2-C3) (36.) ν(C1-C6) (36.) -ν(C1-C6) (6.) ν(C1-C6) (5.)
762.46	732.5716		14.35	ν(C2-H33) (17.) -ν(C1-C6) (13.) -δ(C8-C14-C16) (11.)
743.29	714.153		86.47	δ(C8-C14-C16) (30.) (τ−R2) (12.) ν(C1-C2) (5.) ν(C4-H34) (5.)
736.17	707.3121		33.27	ν(C2-H33) (26.) -ν(C2-H33) (10.) ν(C3-N4) (8.) -ν(C1-H32) (7.) ν(C4-H34) (6.) ν(C2-H33) (5.) ν(C1-C2) (5.)
724.59	696.1861		12.74	ν(C4-H34) (29.) (τ−R2) (18.) ν(C1-C2) (12.) -ν(C3-N4) (7.)
716.1	688.0289		23.91	δ(C8-C14-C16) (21.) ν(C2-H33) (17.) ν(C4-H34) (10.) ν(C2-H33) (9.) ν(C1-C6) (6.) ν(C1-C2) (5.)
706.81	679.103		18.21	ν(C2-H33) (25.) ν(C4-H34) (13.) ν(C1-C6) (11.) -δ(C8-C14-C16) (10.) -ν(C4-C5) (7.) -ν(C1-H32) (5.)
694.6	667.3717		57.73	ν(C2-H33) (18.) -ν(C1-C6) (11.) ν(C4-H34) (8.) -δ(C8-C14-C16) (7.) ν(C4-C5) (7.) -ν(C1-C6) (5.) -ν(C3-C4) (5.) -ν(C1-C2) (5.) (τ−R2) (5.)
682.25	655.5058	667	5.28	ν(C2-H33) (53.) -ν(C1-H32) (32.) -ν(C2-H33) (7.) -ν(C1-C2) (7.)
675.05	648.588		17.19	ν(C4-C5) (12.) -ν(C1-C2) (12.) -ν(C1-C2) (8.) -ν(C4-H34) (7.) ν(C3-N4) (6.) -ν(C2-H33) (5.) ν(C2-H33) (5.)
666.38	640.2579		23.53	δ(C8-C14-C16) (28.) ν(C1-C2) (8.) ν(C1-C6) (5.) ν(C2-C3) (5.) -ν(C3-N4) (5.) 4ν(C2-H33) (5.)
641.16	616.0265		2.66	ν(C2-C3) (14.) -ν(C1-C2) (13.) ν(C4-C5) (8.) ν(C1-H32) (8.) -δ(C8-C14-C16) (7.) ν(C4-C5) (5.)
631.6	606.8413		2.74	ν(C1-C2) (9.) -ν(C4-H34) (7.) ν(C3-N4) (7.) -ν(C2-C3) (7.) -ν(C1-H32) (6.) ν(C2-C3) (6.) ν(C2-H33) (5.) -ν(C1-C2) (5.)

(*continued on next page*)

https://doi.org/10.1016/j.heliyon.2018.e01009

Table 5. (*Continued*)

Wave number unscaled	Wave number scaled	Exp. Wave numbers	Exp.IR$_{int}$	Assignment (PED) ≥ 5 %
630.31	605.6018		1.32	δ(C8-C14-C16) (26.) ν(C2-C3) (24.) -ν(C4-H34) (13.) ν(C4-C5) (6.)
614.96	590.8536		14.97	ν(C1-C6) (23.) -ν(C1-H32) (21.) ν(C2-C3) (19.) -δ(C8-C14-C16) (11.) ν(C2-C3) (5.)
566.24	544.0434		15.77	δ(C8-C14-C16) (20.) -ν(C2-C3) (19.) -ν(C1-H32) (17.) ν(C1-C6) (8.)
537.68	516.6029		1.42	ν(C4-C5) (12.) ν(C1-H32) (10.) -ν(C1-H32) (9.) ν(C2-C3) (5.) ν(C2-H33) (5.) ν(C3C4) (5.) ν(C3N4) (5.)
536.69	515.6518		2.96	ν(C3-N4) (29.) ν(C3-C4) (16.) -ν(C1-H32) (16.) -δ(C8-C14-C16) (6.) ν(C3-N4) (6.) -ν(C3-C4) (5.)
526.12	505.4961		1.36	ν(C3-C4) (25.) ν(C4-H34) (19.) ν(C1-H32) (10.) -ν(C3-N4) (6.) ν(C3-N4) (5.) ν(C5-C6) (5.)
511.3	491.257		3.12	ν(C1-H32) (31.) -ν(C3-N4) (21.) ν(C3-N4) (8.) ν(C1-H32) (5.)
473.04	454.4968		6.53	ν(C1-C6) (21.) -ν(C5-C6) (19.) -ν(C3-C4) (12.) ν(C3-C4) (8.) ν(C4-C5) (7.) -ν(C1-H32) (6.) ν(C4-H34) (5.)
466.85	448.5495		3.89	ν(C1-H32) (21.) -ν(C1-H32) (20.) ν(C3-N4) (13.) ν(C3-N4) (8.)
441.8	424.4814		0.97	ν(C1-H32) (18.) ν(C1-C6) (18.) -ν(C3-N4) (15.) -ν(C3-N4) (6.) -ν(C3-C4) (6.) -ν(C2-H33) (6.)
424.95	408.292		1.2	ν(C3-N4) (33.) ν(C3-C4) (20.) ν(C1-H32) (8.) -(τ−R2) (7.)
422.12	405.5729		1.27	δ(C8-C14-C16) (30.) ν(C1-C2) (25.) -ν(C2-H33) (9.) ν(C3-C4) (5.)

$$E(2) = \Delta E_{ij} = qi\frac{(F_{ij})^2}{(E_j - E_i)} \tag{1}$$

Where, q_i is occupancy of donor orbital; E_i and E_j are diagonal elements; F_{ij} is off diagonal NBO Fock matrix element. The result of the calculations is tabulated in Table 7.

The results showed 22 consecutive high energy transitions in BCOPCA. A transition from π (C_1-C_6) to π* (C_2-C_3) and (C_4-C_5) with stabilization energies of 18.03 and 22.22 kcal mol^{-1}, and an intramolecular charge transfer from π (C_2-C_3) to π* (C_1-C_6) and (C_4-C_5) with stabilisation energies of 21.25 and 18.36 kcal mol^{-1}, designating the presence of conjugation in the phenyl ring attached to the nitrogen atom of pyrrolidine ring. An intramolecular charge transfer from π (C_8-C_{14}) to π* (C_{16}-C_{26}) is seen with an energy of 17.7 kcal mol^{-1}. The molecule also observed four transitions showing intramolecular charge transfer from π (C_{16}-C_{26}) to π* (C_{29}-C_9), (C_8-C_{14}), (C_{22}-C_{23}) and (C_{24}-C_{25}) with stabilisation energies of 56.27, 21.23, 17.82 and 23.43

https://doi.org/10.1016/j.heliyon.2018.e01009

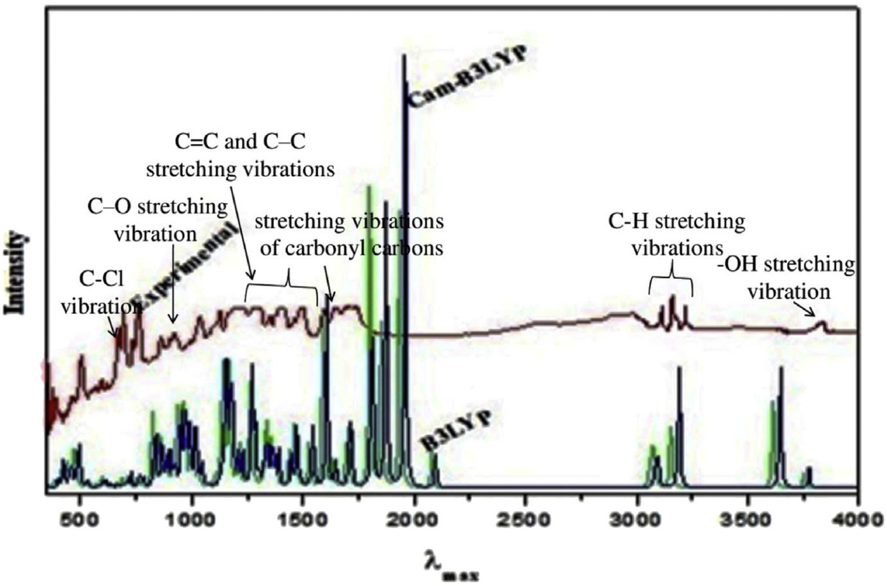

Fig. 7. Comparison between theoretical and experimental IR spectra of BCOPCA.

kcal mol^{-1} respectively. Another intramolecular charge transfer is observed from π (C_{17}-C_{18}) to π* (C_{19}-C_{20}) with a stabilisation energies of 20.40 kcal mol^{-1} and from π (C_{19}-C_{20}) to π* (C_{17}-C_{18}) with a stabilisation energies of 18.42. Charge transfers from π (C_{22}-C_{23}) to π* (C_{16}-C_{26}) and (C_{24}-C_{25}), from π (C_{24}-C_{25}) to π*(C_{22}-C_{23}) and from nonbonding orbital of O_{30} to σ* (C_{26}-H_{47}) with stabilisation energies of 20.12, 18.68 kcal mol^{-1}, 20.18 and 37.82 kcal mol^{-1} are also observed for BCOPCA. Two very high energy transitions from nonbonding orbital of O_{30} and O_{31} to σ* orbitals of (C_{29}-C_9) and (C_9-O_{29}) with stabilisation of 156.15 and 77.29 kcal mol^{-1} are also present in BCOPCA. In BCOPCA charge transfer is also taking place from nonbonding orbital of O_{12} to σ* of (C_{10}-C_{11}) and π* (C_{10}-C_{13}), (C_{17}-C_{18}) with stabilization energies of 19.88 and 77.03, 17.15 kcal mol^{-1}. The intramolecular charge transfer is observed from nonbonding orbital of $Cl_{27and28}$ to σ* (C_{19}-C_{20}) and π* (C_{24}-C_{25}) with a stabilisation energies of 13.74 and 13.07 kcal mol^{-1} respectively. A very high stabilization energy of 38.35 and 26.42 kcal mol^{-1} is due to the charge transfer from nonbonding orbital of N_7 to π* (C_2-C_3) and (C_{11}-O_{12}). All these transitions are due to high delocalisation of bonds inside the molecular system.

3.9. Non -linear optical (NLO) analysis

NLO studies [52, 53] find wide applications in laser technology, optical communication, optical information processing. The results of these studies when performed on BCOPCA (tabulated in Table 8), revealed that the computed dipole moment, polarizability α_{tot} and first hyper polarizability [54] for the BCOPCA are found to be 3.832 D, 66.30814×10^{-24} and 19.477 ×10^{-30} esu for B3LYP functional and 3.994 D, 61.16037×10^{-24} and 16.924 ×10^{-30} esu for CAM-B3LYP functional.

 https://doi.org/10.1016/j.heliyon.2018.e01009

Table 6. The Mulliken charge distribution calculated atB3LYPand CAM-B3LYP/6-31G (d,p) methods of BCOPCA.

Atom no.	Atomic charges (Mulliken)	
	B3LYP/6-31 G (d,p)	**CAM-B3LYP/6-31 G (d,p)**
C_1	−0.0984	−0.112305
C_2	−0.12148	−0.133082
C_3	0.307709	0.298710
C_4	−0.1131	−0.124885
C_5	−0.09443	−0.109076
C_6	−0.08815	−0.108510
N_7	−0.59224	−0.596539
C_8	0.155754	0.160467
C_9	−0.31508	−0.319554
C_{10}	0.003882	−0.006426
C_{11}	0.490942	0.506113
O_{12}	−0.4566	−0.466186
C_{13}	−0.11424	−0.100354
C_{14}	−0.12482	−0.114265
C_{15}	0.127164	0.103231
C_{16}	0.174044	0.152624
C_{17}	−0.11282	−0.117769
C_{18}	−0.09507	−0.109200
C_{19}	−0.0881	−0.092192
C_{20}	−0.10377	−0.116854
C_{21}	−0.01027	−0.015269
C_{22}	−0.13217	−0.140170
C_{23}	−0.08157	−0.094387
C_{24}	−0.10668	−0.113412
C_{25}	−0.087	−0.094325
C_{26}	−0.14349	−0.144029
Cl_{27}	0.00253	−0.016928
Cl_{28}	−0.00293	−0.021647
C_{29}	0.56722	0.554144
O_{30}	−0.50087	−0.512658
O_{31}	−0.46541	−0.470745
H_{32}	0.090539	0.105410
H_{33}	0.123023	0.122702
H_{34}	0.089017	0.106571
H_{35}	0.088672	0.105458

(*continued on next page*)

 https://doi.org/10.1016/j.heliyon.2018.e01009

Table 6. (*Continued*)

Atom no.	Atomic charges (Mulliken)	
	B3LYP/6-31 G (d,p)	CAM-B3LYP/6-31 G (d,p)
H_{36}	0.083435	0.097917
H_{37}	0.206544	0.232032
H_{38}	0.122806	0.142620
H_{39}	0.112816	0.132991
H_{40}	0.096202	0.119416
H_{41}	0.10825	0.124519
H_{42}	0.111383	−0.112305
H_{43}	0.075855	−0.133082
H_{44}	0.086612	0.298710
H_{45}	0.106367	−0.124885
H_{46}	0.140598	−0.109076
H_{47}	0.242209	−0.108510
H_{48}	0.335112	0.596539

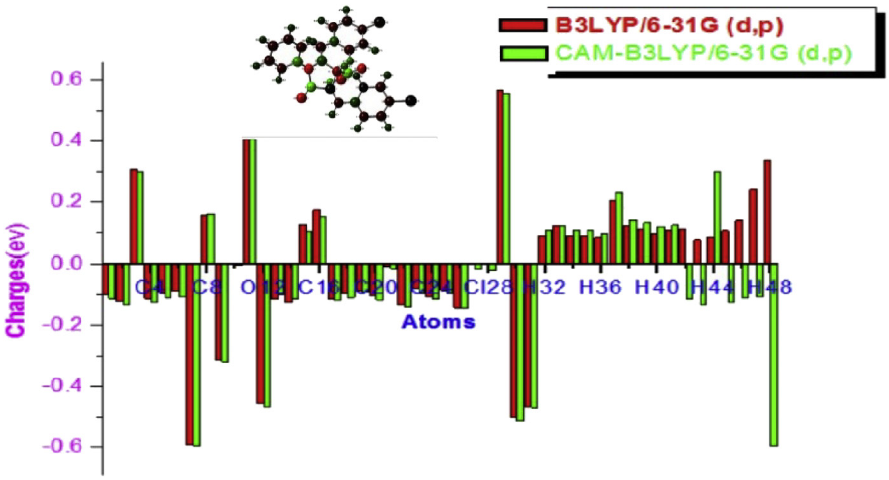

Fig. 8. Mulliken charge distribution in BCOPCA.

3.10. Thermodynamical analysis

Statistical thermodynamic functions mainly heat capacity and entropy were calculated for the molecule at varying temperatures (100−500 K) and summarised in Table 9. The correlation graph between these thermodynamic measurements and temperatures (T) are shown in Figs. 11(a) and (b). The calculated fitting factors (R^2) are 0.998 and 1 for B3LYP and CAM-B3LYP/6-31G (d,p) hybrid functionals respectively. The zero point vibrational energy (ZPVEs), thermal energy, rotational constant, molar heat capacity, entropy and enthalpy at room temperature for

https://doi.org/10.1016/j.heliyon.2018.e01009

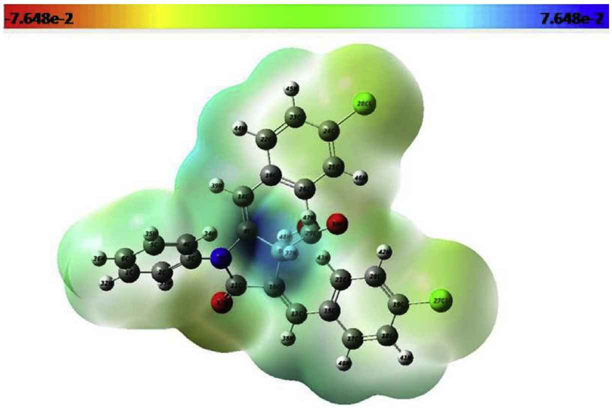

Fig. 9. 3D plot of the molecular electrostatic potential of BCOPCA.

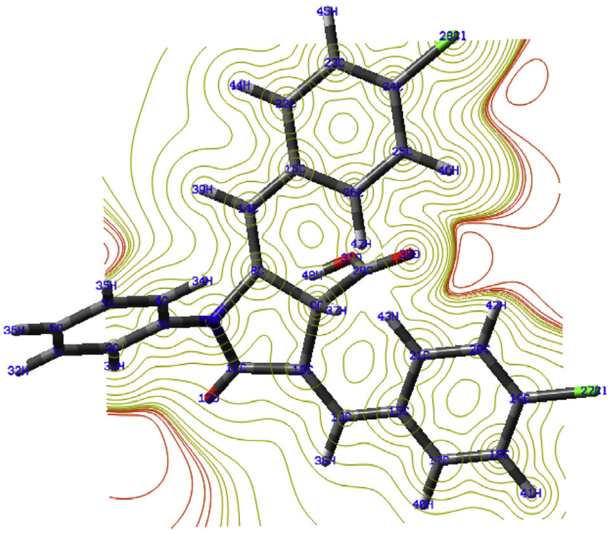

Fig. 10. Electrostatic potential contour surface of BCOPCA.

BCOPCA were obtained and indexed in Table 10 [55, 56]. It is obvious from our observations that the calculated ZPVE energy is lower in B3LYP (225.86 kcal mol^{-1}) than CAM-B3LYP (228.47 kcal mol^{-1}) method. However, the calculated molar heat and entropy were 83.392, 140.86 and 83.029, 140.093 cal mol^{-1} k^{-1} respectively at B3LYP and CAM-B3LYP/6-31G (d,p) hybrid functionals.

3.11. Reactivity descriptors

3.11.1. Global reactivity descriptors

Global reactivity descriptors such as electronegativity, chemical potential (μ), global hardness (η), global softness (S), ΔNmax and electrophilicity index (ω) have been calculated and listed in Table 11. Koopman's theorem was used to confirm chemical reactivity and site selectivity for BCOPCA [56, 57, 58].

https://doi.org/10.1016/j.heliyon.2018.e01009

Table 7. Second order perturbation theory analysis of Fock matrix in NBO basis of BCOPCA.

Doner (i)	Type	ED/e	Acceptor (j)	Type	ED/e	E (2)[a]	(Ej-Ei)[b]	Fij[c]
C1-C6	π	1.66	C2-C3	π*	0.409	18.03	0.28	0.066
C1-C6	π	1.66	C4-C5	π*	0.33	22.22	0.28	0.07
C1-C3	π	1.96	N7-C8	π*	0.044	5.49	1.03	0.068
C2-C3	π	1.62	C1-C6	π*	0.34	21.25	0.29	0.07
C2-C3	π	1.62	C4-C5	π*	0.33	18.36	0.29	0.065
C3-C4	n	1.96	N7-C11	π*	0.119	5.23	1.02	0.067
C4-C5	π	1.69	C1-C6	π*	0.34	18.01	0.29	0.065
C4-C5	π	1.69	C2-C3	π*	0.4	21.69	0.28	0.072
C8-C14	π	1.97	C14-C16	π*	0.025	5.34	1.43	0.073
C8-C14	π	1.97	C16-C26	π*	0.04	17.7	0.33	0.074
C9-C29	σ	1.93	C21-H43	σ*	0.07	8.93	1.23	0.094
C9-C29	σ	1.93	C26-H47	σ*	0.14	38.41	1.34	0.206
C9-H37	σ	1.91	C21-H43	σ*	0.074	14.96	1.07	0.114
C9-H37	σ	1.91	C29-O31	π*	0.12	5.6	0.84	0.062
C10-C13	σ	1.82	C11-O12	π*	0.015	17.43	0.28	0.064
C13-C15	σ	1.96	C10-C13	π*	0.192	5.04	1.4	0.075
C-13-H38	σ	1.96	C9-C10	π*	0.045	7.6	0.9	0.074
C13-H38	σ	1.96	C15-C21	π*	0.035	5.45	1.11	0.07
C14-C16	n	1.96	N7-C8	σ*	0.44	6.73	1.08	0.076
C14-C16	σ	1.96	C8-C14	π*	0.22	5.37	1.39	0.077
C14-C16	σ	1.96	C16-C26	π*	0.44	5.42	1.34	0.076
C14-H39	σ	1.96	C8-H9	σ*	0.049	7.58	0.9	0.074
C14-H39	σ	1.96	C16-C26	π*	0.44	5.48	1.12	0.07
C15-C21	π	1.96	C13-C15	π*	0.024	5.11	1.35	0.074
C16-C26	π	1.96	C14-C16	π*	0.025	5.28	1.35	0.076
C16-C26	π	1.58	C29-C9	π*	0.121	56.27	1.1	0.071
C16-C26	π	1.58	C8-C14	π*	0.22	21.23	0.28	0.065
C16-C26	π	1.58	C22-C23	π*	0.3	17.82	0.28	0.073
C16-C26	π	1.58	C24-C25	π*	0.37	23.43	0.27	0.011
C17-C18	π	1.68	C19-C20	π*	0.37	20.4	0.27	0.067
C19-C20	π	1.66	C17-C18	π*	0.014	18.42	0.3	0.067
C21-C43	σ	1.92	C8-C9	σ*	0.049	6.66	0.91	0.07
C22-C23	π	1.68	C16-C26	π*	0.44	20.12	0.29	0.07
C22-C23	π	1.68	C24-C25	π*	0.377	18.68	0.27	0.06
C24-C25	π	1.68	C16-C26	π*	0.44	15.71	0.31	0.064
C24-C25	π	1.68	C22-C23	π*	0.3	20.18	0.3	0.07
C29-O30	n	1.95	C26-H47	σ*	0.14	37.82	1.73	0.235

(continued on next page)

https://doi.org/10.1016/j.heliyon.2018.e01009

Table 7. (*Continued*)

Doner (i)	Type	ED/e	Acceptor (j)	Type	ED/e	E (2)[a]	(Ej-Ei)[b]	Fij[c]
O31-H48	n	1.98	C29-O30	π*	0.04	8.61	1.31	0.096
LP (1) N7	n	1.62	C2-C3	π*	0.4	38.35	0.3	0.097
LP (1)N7	n	1.62	C11-O12	π*	0.24	26.42	0.26	0.076
LP (1) O12	n	1.97	N7-C11	σ*	0.119	34.24	0.6	0.129
LP (2) O12	n	1.83	C10-C11	σ*	0.072	19.88	0.66	0.105
LP (1) C15	n	1.04	C10-C13	π*	0.192	77.03	0.14	0.12
LP (1) C15	n	1.04	C17-C18	π*	0.29	17.15	0.13	0.106
LP (1) O12	n	0.93	C19-C20	π*	0.37	78.68	0.12	0.108
LP (3) Cl27	π	1.91	C19-C20	σ*	0.37	13.74	0.34	0.066
LP (1) Cl28	π	1.92	C24-C25	π*	0.37	13.07	0.34	0.065
LP (1) O30	n	1.94	C16-C26	π*	0.049	5.47	1.32	0.076
LP (1) O30	n	1.94	C21-H43	σ*	0.074	5.1	0.82	0.06
LP (2) O30	n	1.75	C26-H47	σ*	0.14	22.1	0.92	0.131
LP (2) O30	n	1.75	C29-C9	σ*	0.04	156.15	0.14	0.147
LP (3) O30	n	1.75	C16-C26	π*	0.04	6.32	0.89	0.071
LP (2) O30	n	1.75	C26-H47	σ*	0.14	5.95	0.92	0.068
LP (1) O31	n	1.96	C9-C29	σ*	0.092	7.59	0.95	0.077
LP (2) O31	n	1.79	C9-C29	σ*	0.049	77.29	0.21	0.13

[a] Energy of hyperconjugative interactions (Kcal/mol).
[b] Energy difference between donor and acceptor i and j NBO orbitals in a.u.
[c] The Fock matrix elements between i and j NBO orbitals in a.u.

3.11.2. Local reactivity descriptors

Local reactivity descriptors such as softness (Sk), Fukui Function (FF) and electrophilicity index (ωk) [59, 60] were enumerated in Table 12. Local softnesses (s_k^+, s_k^-,s_k^0) and electrophilicity indices (ω_k^+, ω_k^-, ω_k^0) are described with the help of following equations.

$$s_K^+ = Sf_K^+,\ s_k^- = Sf_K^-,\ s_K^0 = Sf_K^0 \tag{2}$$

$$\omega_K^+ = \omega f_K^+,\ \omega_K^- = \omega f_K^-,\ \omega_K^0 = \omega f_K^0 \tag{3}$$

Where +, −, 0 signs show attack of nucleophile, electrophile and radical.

The observed values at C2, C6, C19, C23 and C25 showed that these sites are more liable to nucleophilic attack whereas the relatively enhanced values at H48, C29, O30, O31 suggested that these sites are accountable for attack of electrophiles. These explorations are helpful enough to provide more information about the chemical reactivity of the molecule.

 https://doi.org/10.1016/j.heliyon.2018.e01009

Table 8. Dipole Moment μ, Polarizability α_{tot} ($\times 10^{-24}$esu) and first order static hyperpolarizability β_{tot} (10^{-30}) data of BCOPCA.

Dipole moment	B3LYP6-31G (d,p)	CAM-B3LYP6-31G (d,p)	Hyperpolarisability	B3LYP 6-31G (d,p)	CAM-B3LYP6-31G (d,p)
μ_x	−3.662	−3.828	β_{xxx}	−2.94566	−18.1538
μ_y	−1.028	−1.081	β_{xxy}	−3.74721	1.572093
μ_z	0.465	0.366	β_{xyy}	15.26366	9.189278
μ	3.832	3.994	β_{yyy}	−4.18332	−2.02151
Polarizability					
α_{xx}	94.94433	86.27759	β_{xxz}	−17.1825	−10.3637
α_{xy}	0.236824	0.337451	β_{xyz}	4.443019	3.289241
α_{yy}	71.67693	67.41914	β_{yyz}	4.662803	−3.53805
α_{xz}	2.720952	3.09738	β_{xzz}	−0.31326	−0.94099
α_{yz}	6.916494	68.98265	β_{yzz}	−0.81097	−0.68121
α_{zz}	32.30315	31.58438	β_{zzz}	−0.08346	0.225054
(α)	66.30814	61.76037	βtotal (esu)	19.477	16.924

3.12. Atom In molecule (AIM) approach

The molecular graph of compound BCOPCA at B3LYP/6-31G (d, p) hybrid functionals is presented in Fig. 12 with help of AIM program. The strong, medium, weak H-bonds and their covalent, partially covalent and electrostatic nature can be denoted by $\nabla^2\rho$(BCP) < 0 and *H*BCP < 0, $\nabla^2\rho$ (BCP) > 0 and *H*BCP < 0 and $\nabla^2\rho$(BCP) > 0 and *H*BCP > 0 [61]. ρ(BCP) and *H*BCP are Laplacian of electron density and total electron density at bond critical point respectively. The various bond interactions and their values are provided in Table 13 and indicated that C2-H24···O12 and C19-H41···O12 are weak interactions having

Table 9. Thermodynamic functions at different temperatures of BCOPCA employing B3LYPand CAM-B3LYP/6-31 G (d,p)methods.

Temperature (T) (K)	B3LYP/6-31-G (d,p)		CAM-B3LYP/6-31-G (d,p)	
	Heat capacity (CV) (Cal/mol K)	Entropy (S) Cal/Mol K)	Heat capacity (CV) (Cal/mol K)	Entropy (S) Cal/Mol K)
100	26.74	86.85	27.35	87.48
200	54.27	115.05	54.74	116.07
298	83.02	142.86	83.39	144.04
300	83.56	143.39	83.93	144.57
400	111.1	171.86	111.54	173.15
500	134.49	199.69	135.08	201.1

https://doi.org/10.1016/j.heliyon.2018.e01009

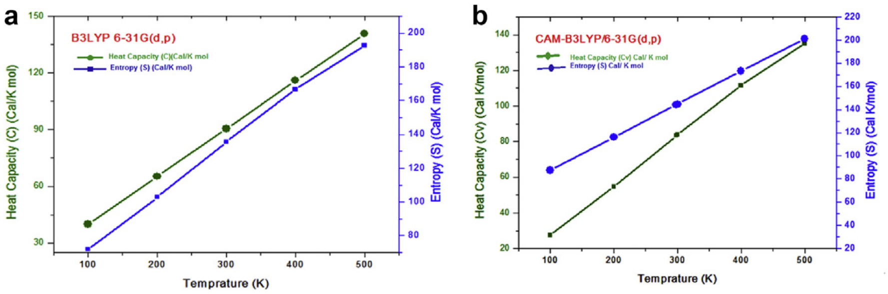

Fig. 11. (a) & (b) Correlation graphs of heat capacity and entropy calculated at various temperatures using B3LYPand CAM-B3LYP/6-31G (d,p) of BCOPCA.

Table 10. Calculated thermodynamic parameters of BCOPCA employing B3LYPand CAM-B3LYP/6-31 G (d,p)methods.

Parameters	B3LYP/6-31 G (d,p)	CAM-B3LYP/6-31 G (d,p)
Zero-point vibrational energy (Kcal/mol)	225.86	228.47
Rotational temperatures (K)	0.00704	0.00704
	0.00482	0.00482
	0.00315	0.00315
Rotational constants (GHZ)		
X	0.14672	0.14672
Y	0.10047	0.10047
Z	0.06559	0.06559
Thermal energy (Kcal/mol)		
Total	238.10	240.85
Translational	0.889	0.889
Rotational	0.889	0.889
Vibrational	236.32	239.07
Molar capacity at constant volume (cal mol^{-1} k^{-1})		
Total	83.392	83.029
Translational	2.9810	2.9810
Rotational	2.9810	2.9810
Vibrational	77.438	77.068
Entropy (cal mol^{-1} k^{-1})		
Total	140.86	140.093
Translational	40.192	44.196
Rotational	37.054	37.052
Vibrational	61.627	62.804

∇^2(BCP) and *H*BCP values greater than zero. The total energy of intramolecular interaction was 0.0903 kcal mol^{-1} as calculated with the help of AIM. There is delocalization of π electrons in aromatic ring as shown by the lower values of ellipticity [62].

 https://doi.org/10.1016/j.heliyon.2018.e01009

Table 11. Calculated ε_{LUMO}, ε_{HOMO}, energy band gap $\varepsilon_{HOMO}-\varepsilon_{LUMO}$, ionization potential (IP), electron affinity (EA), electronegativity (χ), global hardness (η), chemical potential (μ), global electrophilicity index (ω), global softness (S) and additional electronic charge (ΔN_{max}) in eV for BCOPCA, using B3LYP and CAM- B3LYP/6-31G (d,p).

Descriptors	B3LYP/6-31G (d,p)	CAM- B3LYP/6-31G (d,p)
ε_H	−5.4304	−6.6329
ε_L	−2.2490	−1.0993
ε_H-ε_L	−3.1814	−5.5335
IP	5.4304	6.6329
EA	2.2495	1.0993
χ	−3.8399	−3.8661
η	1.5907	2.7667
μ	3.8399	3.8661
ω	4.6344	3.5226
S	0.3143	0.1807
ΔN_{Max}	2.4133	1.3973

3.13. Evaluation of antimicrobial activity

The *in-vitro* antimicrobial activity of BCOPCA was studied using the disc diffusion method with different strains of bacteria [*Salmonella typhi* (St, MTCC 537), *Klebsiella pneumonia* (Kp, MTCC 661), *Pseudomonas aeruginosa* (Pa, MTCC 424)] [63]. Chloroform was used as negative control and Vancomycin was used as standard drug. The zone of inhibition (mm) results showed that compound showed a good bactericidal activity against *Salmonella typhi, Klebsiella pneumonia* and *Pseudomonas aeruginosa* where the diameter of zone of inhibition was 12, 10 and 9.5 mm etc.

3.14. Molecular docking studies

In modern drug designing, molecular docking, which predicts the preferred orientation of one molecule to a second when bound to each other to form a stable complex, is an important tool for understanding drug-receptor interaction. The molecular docking study of BCOPCA was also carried out in the present article to come up with the rationale for the biological activity. All *in silico* docking experiment were carried out the using Auto Dock version 4.2 [64, 65]. Crystal structure of 3-Dehydroquinase from *Salmonella typhi* (PDB ID: 1GQN), Pyridoxal kinase (PDBID: 5B6A) from *Pseudomonas aeruginosa* and Dihydrofolate reductase enzyme from *Klebsiella pneumonia* (PDBID: 4oR7) for the docking studies was downloaded from Protein Data Bank (http://www.rscb.org/pdb).

https://doi.org/10.1016/j.heliyon.2018.e01009

Table 12. Fukui functions (fk^+, fk^-), Local softnesses (sk^+,sk^-) in eV, local electrophilicity indices (ωk+, ωk-) in eV for specific atomic sites of BCOPCA.

Atoms	q_N	q_N+1	q_N-1	f_k+	f_k-	sk^+	sk^-	ωk+	ωk−
1 C	−0.00786	−0.02542	0.033475	−0.01756	−0.04134	−0.00453	−0.01065	−0.06428	−0.15133
2 C	0.001539	0.048247	0.037914	0.046708	−0.03638	0.01204	−0.00937	0.170984	−0.13316
3 C	0.307709	0.009798	0.306242	−0.29791	0.001467	−0.0768	0.000378	−1.09056	0.00537
4 C	−0.02409	0.050011	−0.0047	0.074098	−0.01939	0.019101	−0.005	0.271251	−0.07097
5 C	−0.00575	−0.02706	0.031592	−0.0213	−0.03735	−0.00549	−0.00962	−0.07799	−0.13671
6 C	−0.00471	0.080973	0.055309	0.085687	−0.06002	0.022088	−0.01547	0.313674	−0.21973
7 N	−0.59224	0.102799	−0.57026	0.695039	−0.02198	0.179167	−0.00566	2.544329	−0.08047
8 C	0.155754	−0.04326	0.153809	−0.19901	0.001945	−0.0513	0.000501	−0.72853	0.00712
9 C	−0.10853	0.003445	−0.09773	0.111976	−0.01081	0.028865	−0.00278	0.409911	−0.03956
10 C	0.003882	0.062521	0.002279	0.058639	0.001603	0.015116	0.000413	0.21466	0.005868
11 C	0.490942	−0.01266	0.503595	−0.5036	−0.01265	−0.12982	−0.00326	−1.84354	−0.04632
12 O	−0.4566	−0.01315	−0.42393	0.443457	−0.03267	0.114314	−0.00842	1.623363	−0.1196
13 C	0.008565	0.002923	0.069755	−0.00564	−0.06119	−0.00145	−0.01577	−0.02065	−0.224
14 C	−0.01201	0.071771	0.051188	0.083779	−0.0632	0.021597	−0.01629	0.30669	−0.23134
15 C	0.127164	0.042609	0.134058	−0.08456	−0.00689	−0.0218	−0.00178	−0.30953	−0.02524
16 C	0.174044	−0.01827	0.173628	−0.19232	0.000416	−0.04957	0.000107	−0.70401	0.001523
17 C	−0.01662	−0.02564	0.028202	−0.00903	−0.04482	−0.00233	−0.01155	−0.03305	−0.16406

(*continued on next page*)

https://doi.org/10.1016/j.heliyon.2018.e01009

Table 12. (*Continued*)

Atoms	q_N	q_N+1	q_N-1	f_k+	f_k-	sk^+	sk^-	ωk+	ωk−
18 C	0.013185	0.043672	0.070556	0.030487	−0.05737	0.007859	−0.01478	0.111604	−0.21002
19 C	−0.0881	−0.00617	−0.08513	0.081928	−0.00297	0.021119	−0.00077	0.299914	−0.01088
20 C	0.007614	−0.00083	0.031913	−0.00845	−0.0243	−0.00218	−0.00626	−0.03092	−0.08895
21 C	0.065587	0.054414	0.040768	−0.01117	0.024819	−0.00288	0.006396	−0.0409	0.090855
22 C	−0.04556	0.075571	0.020497	0.121129	−0.06606	0.031225	−0.01702	0.443417	−0.24181
23 C	0.024794	−0.03624	0.085728	−0.06103	−0.06093	−0.01573	−0.0157	−0.22341	−0.22306
24 C	−0.10668	0.052009	−0.10027	0.158684	−0.0064	0.040906	−0.00165	0.580895	−0.02343
25 C	0.053594	−0.00012	0.098318	−0.05372	−0.04472	−0.01385	−0.01153	−0.19663	−0.16372
26 C	−0.14349	0.138092	−0.15236	0.281579	0.008868	0.072585	0.002285	1.030776	0.032463
27 Cl	0.00253	0.001909	0.069687	−0.00062	−0.06716	−0.00016	−0.01731	−0.00227	−0.24584
28 Cl	−0.00293	0.012659	0.081015	0.015591	−0.08395	0.004019	−0.02163	0.057074	−0.3073
29 C	0.809429	0.021538	0.848196	−0.78789	−0.03877	−0.2031	−0.00999	−2.88423	−0.14191
30 O	−0.50087	0.340429	−0.40777	0.841299	−0.0931	0.21687	−0.02399	3.079743	−0.34082
31 O	−0.1303	−0.00657	−0.08558	0.123728	−0.04471	0.031895	−0.01152	0.452931	−0.16368

https://doi.org/10.1016/j.heliyon.2018.e01009

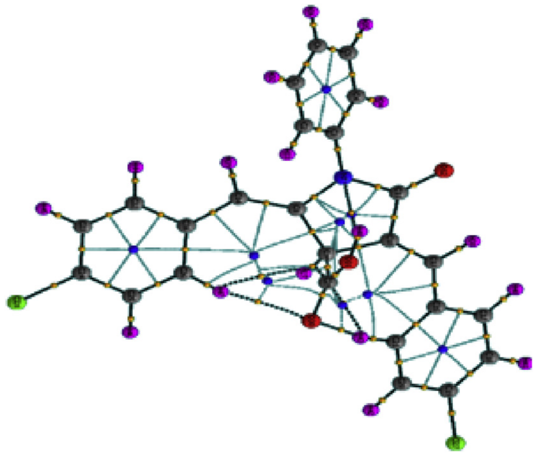

Fig. 12. Molecular graph of BCOPCA using AIM program at B3LYP/6-31G (d,p) level ring critical points (small blue sphere), bond paths (dark green lines).

Table 13. Topological parameters for intramolecular interactions in compound electron density (ρ_{BCP}), Laplacian of electron density ($\nabla^2\rho_{BCP}$), electron kinetic energy density (G_{BCP}), electron potential energy density (V_{BCP}), total electron energy density (H_{BCP}), Hydrogen bond energy (E_{HB}) at bond critical point (BCP).

Interactions	ρ_{BCP}	$\nabla^2\rho_{BCP}$	G_{BCP}	V_{BCP}	H_{BCP}	$E_{HB(Elipticity)}$
C21—H43…O30	0.013730	0.040154	0.009933	−0.009828	0.009734	0.063524
C26—H47…O30	0.011629	0.036157	0.008547	−0.007975	0.016153	0.253943
C31—H48…N7	0.012850	0.041625	0.009642	−0.008877	0.032226	0.430191
C9—H37…H47	0.008698	0.036508	0.006843	−0.004559	0.567843	0.611709

ρ_{BCP}, ∇^2 ρ_{BCP}, G_{BCP}, V_{BCP}, H_{BCP} in a.u. and E_{HB} in (kcal/mol).

The purpose of taking type I DHQase (3-Dehydroquinase), as a target molecule is due to the fact that the shikimate pathway for the biosynthesis of aromatic amino acids (Phenylalanine, Tyrosine and tryptophan), is absent in mammals. Pyridoxal kinase is an essential enzyme for Pyridoxal 5′-phosphate (PLP) homeostasis since PLP is required for the catalytic activity of a variety of PLP-dependent enzymes involved in amino acid, lipid, and sugar metabolism as well as neurotransmitter biosynthesis. Dihydrofolate reductase enzyme is taken as target molecule because the resistance to the antibacterial antifolate trimethoprim (TMP) is increasing in members of the family Enterobacteriaceae including *Klebsiella pneumonia*.

Hydrogen atoms and Kollman charges were added and water molecules were removed from the molecule to execute the docking operations. The B3LYP/6-31G (d,p) functional of theory set was used to prepare minimum energy ligand for docking. Auto Dock requires pre-calculated grid maps. This grid must to include residues of the active site. In the present study the grid size was 60 Å × 60 Å × 60 Å.

https://doi.org/10.1016/j.heliyon.2018.e01009

Lamarckian Genetic Algorithm (LGA) available in Auto Dock was employed for docking. The obtained docking results are stated as correct when the root mean square deviation (RMSD) value is smaller than 2 Ǻ [66]. RMSD is used to estimate the average distance or deviation from the active site of the ligand and most important criterium for the docking results. The binding energy was taken into consideration after the RMSD values, as the molecule may also give lower binding energy with a place other than the active region. UCSF Chimera 1.10.2 program was employed to accomplish graphical representations of the docked pose. The ligand binds at the active site of the protein by H-bonding. Out of 10 conformations acquired by docking into the active site of 3-Dehydroquinase, Pyridoxal kinase and Dihydrofolatereductase, the best conformation was chosen depending on the RMSD value and

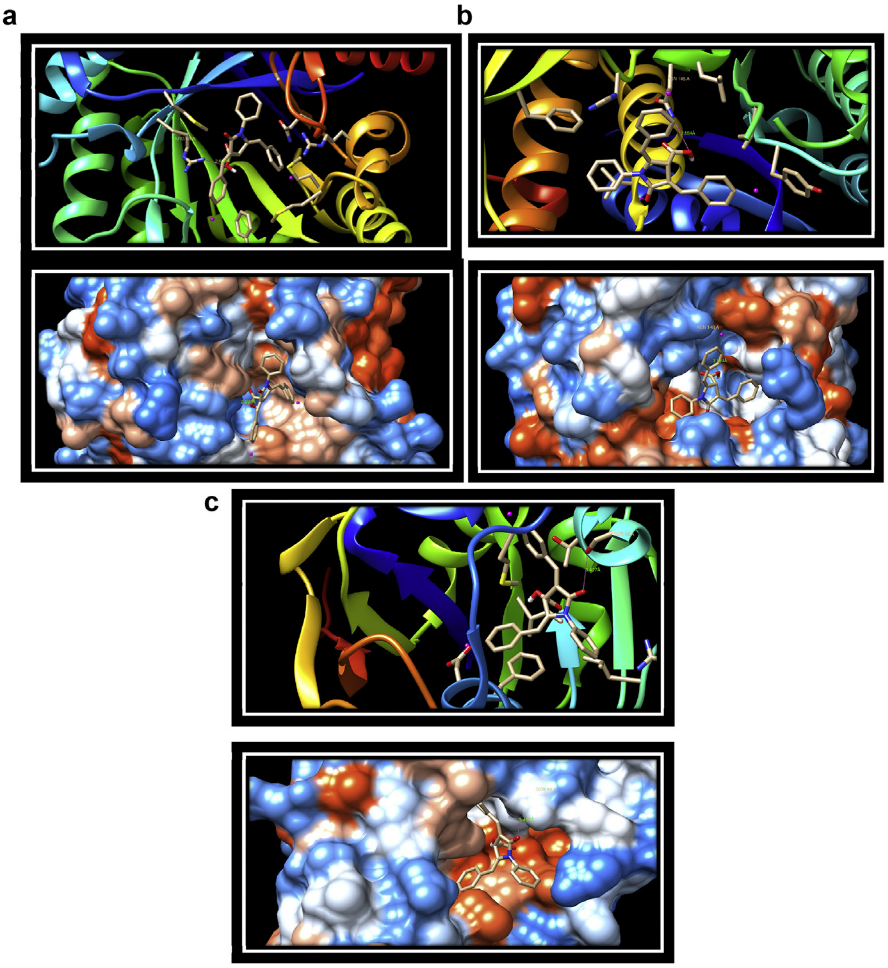

Fig. 13. (a) Schematic representation for the docked conformation at active site of the bacterial enzyme 3-Dehydroquinase (PDB ID: 1GQN) from *Salmonella typhi* with BCOPCA. (b) Schematic representation for the docked conformation at active site of the bacterial enzyme Pyridoxal kinase (PDBID: 5B6A) from *Pseudomonas aeruginosa* with BCOPCA. (c) Schematic representation for the docked conformation at active site of the bacterial enzyme Dihydrofolate reductase (PDBID: 4oR7) enzyme from *Klebsiella pneumonia* with BCOPCA.

 https://doi.org/10.1016/j.heliyon.2018.e01009

binding energy. The ligand-target interaction of BCOPCA to 3-Dehydroquinase, Pyridoxal kinase and Dihydrofolatereductase binding site is depicted in Fig. 13(a–c). The hydrogen bond interactions and binding energy of compound to 3-Dehydroquinase, Pyridoxal kinase and Dihydrofolatereductase are presented in Table 14. Out of all docked conformations, the conformation well bonded to the active site, was chosen for detailed interactions. The docking output inferred that BCOPCA could compactly occupy the active sites of 3-Dehydroquinase, Pyridoxal kinase and Dihydrofolatereductase with binding energy − 2.26, −6.15 and −8.47 kcal/mol respectively.

Estimated Free Energy of Binding for compound with 3-Dehydroquinase = −2.26 kcal mol^{-1} **[=(1)+(2)+(3)-(4)]**

(1) Final Intermolecular Energy = −2.99 kcal mol^{-1}

vdW + Hbond + desolv Energy = −2.41 kcal mol^{-1}

Electrostatic Energy = −0.58 kcal mol^{-1}

(2) Final Total Internal Energy = −0.64 kcal mol^{-1}

(3) Torsional Free Energy = +1.37 kcal mol^{-1}

(4) Unbound System's Energy = +0.00 kcal mol^{-1}

Estimated Free Energy of Binding for compound with Pyridoxal kinase = −6.15 kcal mol^{-1} **[=(1)+(2)+(3)-(4)]**

(1) Final Intermolecular Energy = −7.11 kcal mol^{-1}

vdW + Hbond + desolv Energy = −7.14 kcal mol^{-1}

Electrostatic Energy = +0.03 kcal mol^{-1}

(2) Final Total Internal Energy = −0.41 kcal mol^{-1}

(3) Torsional Free Energy = +1.37 kcal mol^{-1}

(4) Unbound System's Energy = +0.00 kcal mol^{-1}

Table 14. Hydrogen bond interactions of BCOPCA with target 3-Dehydroquinase from *Salmonella typhi* (PDB ID: 1GQN), Pyridoxal kinase (PDBID: 5B6A) from *Pseudomonas aeruginosa* and dihydrofolatereductase enzyme from *Klebsiellapneumoniae* (PDBID: 4oR7).

Macromolecular target	Compound				
	Bonded residue… Ligand atom	No. of hydrogen bonds	Bond distance (Å)	Inhibition constant (μM)	Binding energy Kcal/mol
1GQN	ARG 48…OH	1	2.690	21940	−4.71
5B6A	ASN 148 A…OH	1	3.554	31.09	−6.15
4oR7	SER 49.A…O=C	1	3.427	0.6196	−8.47

https://doi.org/10.1016/j.heliyon.2018.e01009

Estimated Free Energy of Binding for compound with Dihydrofolatereductase = −8.47 kcal mol^{-1} **[=(1)+(2)+(3)-(4)]**

(1) Final Intermolecular Energy = −9.13 kcal mol^{-1}

vdW + Hbond + desolv Energy = −9.51 kcal mol^{-1}

Electrostatic Energy = +0.38 kcal mol^{-1}

(2) Final Total Internal Energy = −0.71 kcal mol^{-1}

(3) Torsional Free Energy = +1.37 kcal mol^{-1}

(4) Unbound System's Energy = +0.00 kcal mol^{-1}

All the three enzymes showed only one hydrogen bond interaction with the best docked conformation of compound. The residue ARG 48 of 3-Dehydroquinase from *Salmonella typhi,* residue ASN 148 A of Pyridoxal kinase (PDBID: 5B6A) from *Pseudomonas aeruginosa* has hydrogen bond interactions with the hydroxyl O atom of ligand at a distance of 2.690 Å and 3.554 Å respectively and residues SER 49 Å of Dihydrofolatereductase enzyme from *Klebsiella pneumonia*, has hydrogen bond interactions with the carbonyl oxygen atom of ligand at a distance of 3.427 Å.

It is a well known fact that, if the number of interactions is greater in the docked complex, it will enrich the bioactivity of the compound but the noteworthy part is that one hydrogen bond interaction was obtained with all three enzymes. Compound may be deemed as a capable inhibitor of 3-Dehydroquinase as compared to Pyridoxal kinase (PDBID: 5B6A) and Dihydrofolatereductase enzyme due to small distance of ligand−residue interaction which was also confirmed by experimental results.

4. Conclusions

The present study gives a detailed account for spectral and computational characterisation of BCOPCA. The complete vibrational analysis of novel (2Z,4Z)-2,4-bis(4-chlorobenzylidene)-5-oxo-1-phenylpyrrolidine-3-carboxylic acid was performed on two different hybrid functionals (B3LYP and CAM-B3LYP6-31G (d,p)).The observed and calculated wavenumbers agreed with each other. The stabilization energy and the calculated HOMO and LUMO energies indicated charge transfer in the molecule, which in turn indicated its bioactive properties. The title compound depicted n → π* HOMO-1 to LUMO+1 with 63% and π → π* HOMO-2 to LUMO with 53% contribution.

The chemical shift values, obtained by GIAO NMR calculations were in good agreement with experimental data. The results of the fundamental vibrational frequencies, calculated with the help of PED, were found satisfactory. The sites of chemical

https://doi.org/10.1016/j.heliyon.2018.e01009

reactivity and charge density distribution of BCOPCA were ascertained by mapping molecular electrostatic potential surface (MESP) and electrostatic potential surface (ESP) contour surface. The MEP and ESP values 7.648 a.u. and −7.648 a.u. indicated that C11, O12 and C47, O30 are most preferred sites for electrophilic and nucleophilic attack. The delocalisation of π electrons in the aromatic ring is shown by the lower values of ellipticity and four feeble hydrogen bonds were explored by AIM approach. IR showed good agreement between experimental and calculated value. Mulliken charge distribution confirmed the enhanced value of charge on H48 that can be accounted to hydrogen bonding. Molecular docking studies using *in-silico* analysis were done to access the interactions of BCOPCA with 3-Dehydroquinase (PDB ID: 1GQN), Pyridoxal kinase (PDBID: 5B6A) and Dihydrofolate reductase (PDBID: 4oR7) enzymes from *Salmonella typhi, Pseudomonas aeruginosa* and *Klebsiella pneumonia* and matched well with the *in vitro* antibacterial activity.

Declarations

Author contribution statement

Poornima Devi: performed the experiments.

Shaheen Fatma, Shraddha Shukla, Roop Kumar, Vineeta Singh: contributed reagents, materials, analysis tools or data.

Abha Bishnoi: conceived and designed the experiments; wrote the paper.

Funding statement

This research did not receive any specific grant from funding agencies in the public, commercial, or not-for-profit sectors.

Competing interest statement

The authors declare no conflict of interest.

Additional information

No additional information is available for this paper.

Acknowledgements

Authors are thankful to the Head, Department of Chemistry, Lucknow University, Lucknow, for providing laboratory, spectral and computational facilities.

https://doi.org/10.1016/j.heliyon.2018.e01009

References

[1] H.B. John, M.B. John, Wilson and Gisvold's Textbook of Organic Medicinal and Pharmaceutical Chemistry, eleventh ed., Lippincott Williams and Wilkins, Philadelphia, 2004, p. 1.

[2] X. Li, Y. Li, W. Xu, Design, synthesis, and evaluation of novel galloyl pyrrolidine derivatives as potential anti-tumor agents, Bioorg. Med. Chem. 14 (2006) 1287−1293.

[3] B. Malawska, New anticonvulsant agents, Curr. Top. Med. Chem. 5 (2005) 69−85.

[4] D.G. Barrett, J.G. Catalano, D.N. Deaton, A.M. Hassell, S.T. Long, A.B. Miller, et al., Novel, potent P2-P3 pyrrolidine derivatives of ketoamide-based cathepsin K inhibitors, Bioorg. Med. Chem. Lett. 16 (2006) 1735−1739.

[5] J.A. Tran, C.W. Chen, W. Jiang, F.C. Tucci, B.A. Fleck, et al., Pyrrolidines as potent functional agonists of the human melanocortin-4 receptor, Bioorg. Med. Chem. Lett. 17 (2007) 5165−5170.

[6] I. Hamlaoui, R. Bencheraiet, R. Bensegueni, M. Bencharif, Experimental and theoretical study on DPPH radical scavenging mechanism of some chalcone quinoline derivatives, J. Mol. Struct. 1156 (2018) 385−389.

[7] A.K. Verma, A. Bishnoi, S. Fatma, Synthesis, spectral analysis and quantum chemical studies on molecular geometry, J. Mol. Struct. 1116 (2016) 9−21.

[8] S. Fatma, A. Bishnoi, A.K. Verma, V. Singh, K. Srivastava, Quantum chemical calculations and molecular docking studies of 5-(4-chlorobenzylidene) thiazolidine-2,4-dione(CTD) and its mannich product 5-(4-chlorobenzylidene)-3-(morpholinomethyl)thiazolidine-2,4-dione (CMTD), J. Mol. Struct. 1157 (2018) 177−190.

[9] A.P. Scott, L. Radom, Harmonic vibrational frequencies: an evaluation of Hartree-Fock, Møller-Plesset, quadratic configuration interaction, density functional theory, and semiempirical scale factors, J. Phys. Chem. 100 (1996) 16502−16513.

[10] E.J. Ocola, T. Brito, K. McCann, J. Laane, Conformational energetics and low-frequency vibrations of cyclohexene and its oxygen analogs, J. Mol. Struct. 978 (2010) 74−78.

[11] J.R. Durig, A. Ganguly, A.M. El Defrawy, G.A. Guirgis, T.K. Gounev, W.A. Herrebout, B.J. Van Der Veken, Conformational stability, r0 structural

https://doi.org/10.1016/j.heliyon.2018.e01009

parameters, barriers to internal rotation and vibrational assignment of cyclobutylamine, J. Mol. Struct. 918 (2009) 64–76.

[12] J.R. Durig, A. Ganguly, A.M. El Defrawy, T.K. Gounev, G.A. Guirgis, Conformational stability of cyclobutanol from temperature dependent infrared spectra of xenon solutions, r0 structural parameters, ab initio calculations and vibrational assignment, Spectrochim. Acta A 71 (2008) 1379–1389.

[13] Ö. Alver, C. Parlak, Vibrational spectroscopic investigation and conformational analysis of 1-pentylamine: a comparative density functional study, J. Theor. Comput. Chem. 9 (2010) 667–685.

[14] E. Güneş, C. Parlak, DFT, FT-Raman and FT-IR investigations of 5-methoxysalicylic acid, Spectrochim. Acta A 82 (2011) 504–512.

[15] L.P. Paytash, E. Sparrow, J.C. Gathe, The reaction of itaconic acid with primary amines, J. Am. Chem. Soc. 72 (1950) 1415–1416.

[16] W. Kohn, A.D. Becke, R.G. Parr, Density functional theory of electronic structure, J. Phys. Chem. 100 (1996) 12974–12980.

[17] C. Lee, W. Yang, R.G. Parr, Development of the Colle-Salvetti correlation-energy formula into a functional of the electron density, Phys. Rev. B37 (1988) 785–789.

[18] M.J. Frisch, G.W. Trucks, H.B. Schlegel, G.E. Scuseria, M.A. Robb, J.R. Cheeseman, G. Scalmani, V. Barone, B. Mennucci, G.A. Petersson, H. Nakatsuji, M. Caricato, X. Li, H.P. Hratchian, A.F. Izmaylov, J. Bloino, G. Zheng, J.L. Sonnenberg, M. Hada, M. Ehara, K. Toyota, R. Fukuda, J. Hasegawa, M. Ishida, T. Nakajima, Y. Honda, O. Kitao, H. Nakai, T. Vreven, J.A. Montgomery Jr., J.E. Peralta, F. Ogliaro, M. Bearpark, J.J. Heyd, E. Brothers, K.N. Kudin, V.N. Staroverov, R. Kobayashi, J. Normand, K. Raghavachari, A. Rendell, J.C. Burant, S.S. Iyengar, J. Tomasi, M. Cossi, N. Rega, J.M. Millam, M. Klene, J.E. Knox, J.B. Cross, V. Bakken, C. Adamo, J. Jaramillo, R. Gomperts, R.E. Stratmann, O. Yazyev, A.J. Austin, R. Cammi, C. Pomelli, J.W. Ochterski, R.L. Martin, K. Morokuma, V.G. Zakrzewski, G.A. Voth, P. Salvador, J.J. Dannenberg, S. Dapprich, A.D. Daniels, Ö. Farkas, J.B. Foresman, J.V. Ortiz, J. Cioslowski, D.J. Fox, Gaussian 09, Revision A.1, Gaussian Inc., Wallingford CT, 2009.

[19] K. Wolinski, J.F. Hinton, P. Pulay, Efficient implementation of the gauge-independent atomic orbital method for NMR chemical shift calculations, J. Am. Chem. Soc. 112 (1990) 8251–8260.

 https://doi.org/10.1016/j.heliyon.2018.e01009

[20] E.D. Glendening, J.K. Badenhoop, A.E. Reed, J.E. Carpenter, J.A. Bohmann, C.M. Morales, F. Weinhold, NBO 5.0, Theoretical Chemistry Institute, University of Wisconsin, Madison, 2001.

[21] R.F.W. Bader, J.R. Cheeseman, AIMPAC, 2000.

[22] J.M.L. Martin, C. Van Alsenoy, GAR2PED, A Program to Obtain a Potential Energy Distribution from a Gaussian Archive Record, University of Antwerp, Belgium, 1995.

[23] P. Devi, S. Fatma, H. Parveen, A. Bishnoi, R. Singh, Spectroscopic analysis, first order hyperpolarizability, NBO, HOMO and LUMO analysis of 5-oxo-1-phenylpyrrolidine-3-carboxylic acid: experimental and theoretical approach, Indian J. Pure Appl. Phys. 56 (2018) 814–829.

[24] H. Karapetyan, R. Tamazyan, A. Martirosyan, V. Hovhannesyan, S. Gasparyan, 1-Substituted derivatives of 2-aryl-5-oxopyrrolidine-2-carboxylic acid, Acta Cryst. C58 (2002) o399–o401.

[25] V. Arjunan, P. Ravindran, T. Rani, S. Mohan, FTIR, FT-Raman, FT-NMR, *ab initio* and DFT electronic structure investigation on 8-chloroquinoline and 8-nitroquinoline, J. Mol. Struct. 988 (2011) 91–101.

[26] M. Cossi, V. Barone, Time-dependent density functional theory for molecules in liquid solutions, J. Chem. Phys. 115 (2001) 4708–4717.

[27] Y. Hiroshi, E. Akito, Density functional vibrational analysis using wavenumber-linear scale factors, Chem. Phys. Lett. 325 (2000) 477–483.

[28] N.B. Colthup, L.H. Daly, S.E. Wiberley, Introduction to Infrared and Raman spectroscopy, Academic Press, New York, 1990.

[29] J.H.S. Green, D.J. Harrison, W. Kynaston, Vibrational spectra of benzene derivatives—XIV: mono substituted phenols, Spectrochim. Acta A 27 (1971) 2199–2217.

[30] E.T.G. Lutz, J.H.V. Mass, Spectrochim. Acta A 42 (1986) 749.

[31] D.N. Sathyanarayana, in: Vibrational Spectroscopy Theory and Applications, second ed., New Age International(P) Ltd. Publishers, New Delhi, 2004.

[32] P.B. Nagabalasubramanian, S. Periandy, S. Mohan, M. Govindarajan, FTIR and FT Raman spectra, vibrational assignments, ab initio, DFT and normal coordinate analysis of α,α dichlorotoluene, Spectrochim. Acta A 73 (2009) 277–280.

[33] G. Varsanyi, Assignments for Vibrational Spectra of Seven Hundred Benzene Derivatives, vols. 1 and 2, Academiai Kiado, Budapest, 1973.

https://doi.org/10.1016/j.heliyon.2018.e01009

[34] C. Arunagiri, M. Arivazhagan, A. Subashini, Vibrational spectroscopic (FT-IR and FT-Raman), first-order hyperpolarizablity, HOMO, LUMO, NBO, Mulliken charges and structure determination of 2-bromo-4-chlorotoluene, Spectrochim. Acta A 79 (2011) 1747−1756.

[35] V. Krishnakumar, R. John Xavier, Normal coordinate analysis of vibrational spectra of 2-methylindoline and 5-hydroxyindane, Indian J. Pure. Appl. Phys. 41 (2003) 95−99. http://hdl.handle.net/123456789/25035.

[36] A. Altun, K. Gölcük, M. Kumru, Theoretical and experimental studies of the vibrational spectra of m-methylaniline, J. Mol. Struct. (Theochem) 625 (2003) 17−24.

[37] T. Harayama, A. Hori, G. Serban, Y. Morikami, T. Matsumoto, H. Abe, Y. Takeuchi, Concise synthesis of quinazoline alkaloids, luotonins A and B, and rutaecarpine, Tetrahedron 60 (2004) 10645−10649.

[38] K. Drużbicki, E. Mikuli, M.D. Ossowska-Chruściel, Experimental (FT-IR, FT-RS) and theoretical (DFT) studies of vibrational dynamics and molecular structure of 4-n-pentylphenyl-4′-n-octyloxythiobenzoate (8OS5), Vib. Spectrosc. 52 (2010) 54−62.

[39] D. Dołęga, A. Migdal-Mikulo, J. Chruściel, Experimental (FT-IR, FT-RS) and theoretical (DFT) studies of vibrational dynamics and molecular structure of 4-n-pentylphenyl-4’-n-heptyloxythiobenzoate (7OS5), J. Mol. Struct. 933 (2009) 30−37.

[40] V.K. Rastogi, M.A. Palafox, K. Lang, S.K. Singhal, R.K. Soni, R. Sharma, Vibrational spectra and thermodynamics of biomolecule: 5-chlorocytosine, Indian J. Pure Appl. Phys. 44 (2006) 653−660. http://hdl.handle.net/123456789/8355.

[41] M. Govindarajan, M. Karabacak, Spectroscopic properties, NLO, HOMO-LUMO and NBO analysis of 2,5-lutidine, Spectrochim. Acta Part A 96 (2012) 421−435.

[42] S. Ramalingam, M. Karabacak, S. Periandy, D. Tanuja, Spectroscopic (infrared, Raman, UV and NMR) analysis, Gaussian hybrid computational investigation (MEP maps/HOMO and LUMO) on cyclohexanone oxime, Spectrochim. Acta Part A 96 (2012) 207−220.

[43] S. Ramalingan, S. Periandy, M. Govindarajan, S. Mohan, FTIR and FT Raman spectra, assignments, ab initio HF and DFT analysis of 4-nitrotoluene, Spectrochim. Acta Part A 75 (2010) 1308−1314.

 https://doi.org/10.1016/j.heliyon.2018.e01009

[44] N. Prabavathi, N. Senthil Nayaki, The spectroscopic (FT-IR, FT-Raman and NMR), first order hyperpolarizability and HOMO–LUMO analysis of 2-mercapto-4(3H)-quinazolinone, Spectrochim. Acta Part A Mol. Biomol. Spectrosc. 129 (2014) 572–583.

[45] S. Fatma, A. Bishnoi, A.K. Verma, Synthesis, spectral analysis (FT-IR, 1H NMR, 13C NMR and UV–visible) and quantum chemical studies on molecular geometry, NBO, NLO, chemical reactivity and thermodynamic properties of novel 2-amino-4-(4-(dimethylamino)phenyl)-5-oxo-6-phenyl-5,6-dihydro-4H-pyrano[3,2-c]quinoline-3-carbonitrile, J. Mol. Struct. 1095 (2015) 112–124.

[46] R.N. Singh, A. Kumar, R.K. Tiwari, P. Rawat, Synthesis, molecular structure, hydrogen-bonding, NBO and chemical reactivity analysis of a novel 1,9-bis(2-cyano-2-ethoxycarbonylvinyl)-5-(4-hydroxyphenyl)-dipyrromethane: a combined experimental and theoretical (DFT and QTAIM) approach, Spectrochim. Acta Part A Mol. Biomol. Spectrosc. 113 (2013) 378–385.

[47] S. Zaater, A. Bouchoucha, S. Djebbar, M. Brahimi, Structure, vibrational analysis, electronic properties and chemical reactivity of two benzoxazole derivatives: functional density theory study, J. Mol. Struct. 1123 (2016) 344–354.

[48] S.K. Saha, A. Hens, N.C. Murmu, P. Banerjee, A comparative density functional theory and molecular dynamics simulation studies of the corrosion inhibitory action of two novel N-heterocyclic organic compounds along with a few others over steel surface, J. Mol. Liq. 215 (2016) 486–495.

[49] P. Politzer, J.S. Murray, Electrostatic potential analysis of dibenzo-p-dioxins and structurally similar systems in relation to the or biological activities, in: D.L. Beveridge, R. Lavery (Eds.), Theoretical Biochemistry and Molecular Biophysics: A Comprehensive Survey, Protein, vol. 2, Adenine Press, Schenectady, NY, 1991 (Chapter 13).

[50] E.D. Glendening, A.E. Reed, J.E. Carpenter, F. Weinhold, NBO Version 3.1, TCI, University of Wisconsin, Madison, 1998.

[51] A.E. Reed, L.A. Curtis, F. Weinhold, Intermolecular interactions from a natural bond orbital, donor-acceptor viewpoint, Chem. Rev. 88 (1988) 899–926.

[52] C. Andraud, T. Brotin, C. Garcia, F. Pelle, P. Goldner, B. Bigot, A. Collet, Theoretical and experimental investigations of the nonlinear optical properties of vanillin, polyenovanillin, and bisvanillin derivatives, J. Am. Chem. Soc. 116 (1994) 2094–2102.

[53] V.M. Geskin, C. Lambert, J.L. Bredas, Origin of high second- and third-order nonlinear optical response in ammonio/borato diphenylpolyene zwitterions:

 https://doi.org/10.1016/j.heliyon.2018.e01009

the remarkable role of polarized aromatic groups, J. Am. Chem. Soc. 125 (2003) 15651–15658.

[54] D.A. Kleinman, Nonlinear dielectric polarization in optical media, Phys. Rev. 126 (1962) 1977–1979.

[55] E. Gopinath, R. John Xavier, Quantum chemical calculations, vibrational studies, HOMO–LUMO and NBO/NLMO analysis of 2-bromo-5-nitrothiazole, Spectrochim. Acta Part A 104 (2013) 394–402.

[56] M. Arivazhagan, J. Senthilkumar, Molecular structure, vibrational spectral assignments, HOMO-LUMO, MESP, Mulliken analysis and thermodynamic properties of 2,6-xylenol and 2,5-dimethyl cyclohexanol based on DFT calculation, Spectrochim. Acta Part A Mol. Biomol. Spectrosc. 137 (2015) 490–502.

[57] S.M. Soliman, M. Hagar, F. Ibid, E. Sayed, H.E. Ashry, Experimental and theoretical spectroscopic studies, HOMO-LUMO, NBO analyses and thione-thiol tautomerism of a new hybrid of 1,3,4-oxadiazole-thione with quinazolin-4-one, Spectrochim. Acta Part A Mol. Biomol. Spectrosc. 145 (2015) 270–279.

[58] A. Sethi, R. Prakash, Novel synthetic ester of brassicasterol, DFT investigation including NBO, NLO response, reactivity descriptor and its intramolecular interactions analyzed by AIM theory, J. Mol. Struct. 1083 (2015) 72–81.

[59] R.G. Parr, L. Szentpaly, S. Liu, Electrophilicity index, J. Am. Chem. Soc. 121 (1999) 1922–1924.

[60] K. Chattaraj, S. Giri, Stability, reactivity, and aromaticity of compounds of a multivalent superatom, J. Phys. Chem. A 111 (2007) 11116–11121.

[61] E. Espinosa, E. Molins, C. Lecomte, Hydrogen bond strengths revealed by topological analyses of experimentally observed electron densities, Chem. Phys. Lett. 285 (1998) 170–173.

[62] L.F. Matta, R.J. Boyd, An Introduction of the Quantum theory of Atom in Molecule, Wiley-VCH Verlag Gmbh, 2007.

[63] National Committee for Clinical Laboratory Standards, Approved standard M7-A5 Methods for dilution antimicrobial susceptibility, fourth ed., NCCLS, Wayne, PA, 2000.

[64] R. Huey, G.M. Morris, A.J. Olson, D.S. Goodsell, A semiempirical free energy force field with charge-based desolvation, J. Comp. Chem. 28 (2007) 1145–1152.

 https://doi.org/10.1016/j.heliyon.2018.e01009

[65] O. Trott, A. Olson, AutoDock Vina: improving the speed and accuracy of docking with a new scoring function, efficient optimization and multithreading, J. Comp. Chem. 31 (2010) 455–461.

[66] B. Kramer, M. Rarey, T. Lengauer, Evaluation of the FLEXX incremental construction algorithm for protein–ligand docking, Proteins Struct. Funct. Bioinf. 37 (1999) 228.

 https://doi.org/10.1016/j.heliyon.2018.e01009